iScience

Article

Exploiting the therapeutic vulnerability of IDH-mutant gliomas with zotiraciclib

Graphical abstract

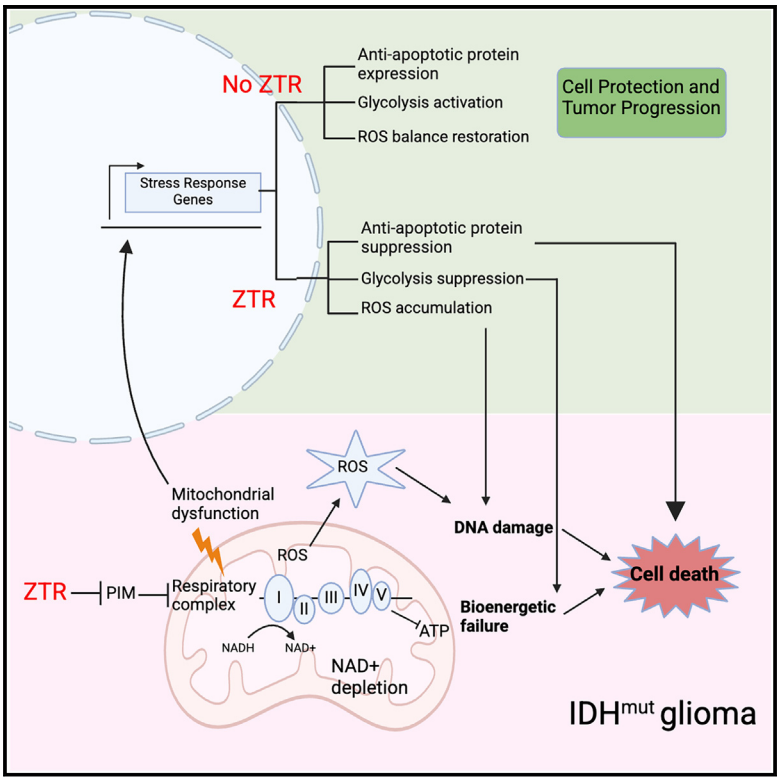

Highlights

- Zotiraciclib (ZTR), a CDK9 inhibitor, hinders IDH-mutant glioma growth *in vitro* and *in vivo*
- ZTR induces apoptosis and DNA damage, resulting in cell death in IDH-mutant cells
- ZTR inhibits PIM kinases, triggering mitochondrial stress and causing bioenergetic failure
- These findings led to the clinical trial NCT05588141 evaluating ZTR for IDH-mutant gliomas

Authors

Ying Pang, Qi Li, Zach Sergi, ..., Maria G. Castro, Taranjit S. Gujral, Jing Wu

Correspondence

jing.wu3@nih.gov

In brief

Therapeutics; Cancer

Pang et al., 2025, iScience *28*, 112283
April 18, 2025 Published by Elsevier Inc.
https://doi.org/10.1016/j.isci.2025.112283

CellPress

iScience

CellPress
OPEN ACCESS

Article

Exploiting the therapeutic vulnerability of IDH-mutant gliomas with zotiraciclib

Ying Pang,[1] Qi Li,[1] Zach Sergi,[1] Guangyang Yu,[1] Olga Kim,[1] Peng Lu,[1] Marina Chan,[2] Xueyu Sang,[1] Herui Wang,[1] Alice Ranjan,[1] Robert W. Robey,[3] Ferri Soheilian,[4] Bao Tran,[5] Felipe J. Núñez,[6] Meili Zhang,[1] Hua Song,[1] Wei Zhang,[1] Dionne Davis,[1] Mark R. Gilbert,[1] Michael M. Gottesman,[3] Zhenggang Liu,[7] Craig J. Thomas,[8] Maria G. Castro,[6] Taranjit S. Gujral,[2] and Jing Wu[1,9,*]

[1]Neuro-Oncology Branch, Center for Cancer Research, National Cancer Institute, National Institutes of Health, Bethesda, MD 20892, USA
[2]Human Biology Division, Fred Hutchinson Cancer Center, Seattle, WA 98109, USA
[3]Laboratory of Cell Biology, National Cancer Institute, National Institutes of Health, Bethesda, MD 20892, USA
[4]Electron Microscopy Laboratory, Center for Cancer Research, National Cancer Institute, National Institutes of Health, Frederick, MD 21701, USA
[5]Cancer Research Technology Program, Center for Cancer Research, National Cancer Institute, Frederick, MD 20701, USA
[6]Departments of Neurosurgery and Cell and Developmental Biology, University of Michigan Medical School, Ann Arbor, MI 48109, USA
[7]Laboratory of Immune Cell Biology, Center for Cancer Research, National Cancer Institute, National Institutes of Health, Bethesda, MD 20892, USA
[8]Division of Pre-Clinical Innovation, National Center for Advancing Translational Sciences (NCATS), National Institutes of Health, Rockville, MD 20850, USA
[9]Lead contact
*Correspondence: jing.wu3@nih.gov
https://doi.org/10.1016/j.isci.2025.112283

SUMMARY

Isocitrate dehydrogenase (IDH)-mutant gliomas have distinctive metabolic and biological traits that potentially render them susceptible to targeted treatments. Here, by conducting a high-throughput drug screen, we pinpointed a specific vulnerability of IDH-mutant gliomas to zotiraciclib (ZTR). ZTR exhibited selective growth inhibition across multiple IDH-mutant glioma *in vitro* and *in vivo* models. Mechanistically, ZTR at low doses suppressed CDK9 and RNA Pol II phosphorylation in IDH-mutant cells, disrupting mitochondrial function and NAD+ production, resulting in oxidative stress. Integrated biochemical profiling of ZTR kinase targets and transcriptomics unveiled that ZTR-induced bioenergetic failure was linked to the suppression of PIM kinase activity. We posit that the combination of mitochondrial dysfunction and an inability to adapt to oxidative stress resulted in significant cell death upon ZTR treatment, ultimately increasing the therapeutic vulnerability of IDH-mutant gliomas. These findings prompted a clinical trial evaluating ZTR in IDH-mutant gliomas (NCT05588141).

INTRODUCTION

Treating diffuse gliomas poses an immense challenge due to the intertumor heterogeneity and the limited availability of effective drugs that can sufficiently penetrate the blood-brain barrier (BBB). Level I evidence from a previous clinical trial indicates diverse clinical responses to the same treatment among various subsets of histologically similar but molecularly distinct gliomas.[1] This underscores the importance of treating glioma subsets based on their unique molecular characterization associated tumor biology and overall therapeutic vulnerability to achieve improved clinical outcomes.

The *IDH* mutation is a crucial genetic feature found in a subset of adult diffuse gliomas, and the mutation status is used as a key biomarker in the WHO classification of diffuse gliomas.[2] Wild-type IDH converts isocitrate to a-ketoglutarate, generating NADPH, while the IDH-mutant enzyme produces the oncometabolite 2-hydroxyglutarate (2-HG) and consumes NADPH.[3,4] Due to the accumulation of 2-HG and depletion of NADPH, IDH-mutant gliomas exhibit distinct biological characteristics, including redox imbalance, altered DNA damage repair, and heightened reliance on mitochondrial function for ATP production.[5–7] These unique features of create potential vulnerabilities to specific drugs that modulate tumor metabolism. Building upon the promising clinical activity of zotiraciclib (ZTR) and a mechanistic rationale for targeting glioma vulnerability, we aimed to investigate the selective application of ZTR in gliomas harboring *IDH* mutations.

ZTR, also called TG02, a pyrimidine-based multi-kinase inhibitor, primarily inhibits cyclin-dependent kinase 9 (CDK9), regulating transcriptional processes in multiple cancer cell models.[8] Previous clinical trials have investigated ZTR and demonstrated its safety profiles in cancer patients.[9,10] Our previous studies have shown that ZTR modulates various mechanisms of cancer cell survival in glioblastomas.[11] ZTR suppresses transcriptional process, induces mitochondrial dysfunction, depletes cellular

ATP, and leading to cell death in glioblastoma. Importantly, *in vivo* experiments provided evidence to support the ability of ZTR to penetrate the BBB, a prerequisite for targeting gliomas.[11] Based on the promising preclinical and clinical evidence, the US Food and Drug Administration (FDA) granted orphan drug designation to ZTR as a therapy for malignant gliomas. Preliminary analysis of clinical outcomes revealed a statistically significant improvement in progression-free survival of patients with IDH-mutant gliomas compared to those with IDH-wildtype gliomas. While the generally favorable prognosis of IDH-mutant gliomas may contribute to this improved treatment response, the observed improved responses could also indicate a potential therapeutic vulnerability in this subset of gliomas.

This study aims to explore preclinical evidence of selective sensitivities to ZTR in IDH-mutant gliomas and unravel the mechanisms behind this therapeutic vulnerability to ZTR. The ability of ZTR to penetrate the BBB and its effectiveness could justify its use as a therapeutic strategy for IDH-mutant gliomas. While our previous study demonstrated that the combined ZTR and TMZ improved survival in preclinical glioblastoma models, overlapping toxicities were also observed in the clinical studies. If therapeutic vulnerability to ZTR is confirmed in preclinical studies of IDH-mutant glioma, it may lead to effective tumor control with reduced toxicity from combined treatment.

RESULTS

Zotiraciclib has superior efficacy in IDH-mutant glioma cells

To demonstrate the superior efficacy of ZTR in IDH-mutant gliomas, we evaluated the cell viability of a panel of glioma cells with and without *IDH* mutations after ZTR treatment. First, using primary patient-derived glioma stem-like cell (GSC) models that have been cultivated in 3D environment, we observed a lower half maximal inhibition concentration (IC_{50}) of ZTR in IDH-mutant cells (TS603 = 7.06 nM, BT142 = 9.00 nM), compared to IDH-wildtype cells (GSC923 = 31.95 nM, GSC827 = 23.53 nM) (Figure 1A). In order to investigate the selective sensitivity to ZTR across various IDH-mutant cells, a fibrosarcoma cell line HT1080 was included, exhibited a lower IC_{50} of 35.94 nM compared to 66.13 nM in U251, a patient-derived IDH-wildtype cell line growing in a similar culture environment when treated with ZTR (Figure 1B). Furthermore, we assessed the ZTR IC_{50} in mouse and patient-derived isogenic cell lines (NPA (*shp53/shATRX/wtIDH1*)30.73 nM; NPAI ((*shp53/shATRX/mIDH1*^{R132H}), 17.65 nM, and GBM1-wildtype = 23.13 nM/GBM1-mutant = 16.95 nM) (Figure 1C). An additional genetically engineered isogenic cell model using single base editing of a patient-derived glioblastoma cell was tested against ZTR as well (Figure S1A). Consistently, IDH-mutant cells displayed a lower IC_{50} compared to the isogenic IDH-wildtype cells, indicating an increased sensitivity to ZTR in the IDH-mutant cells. *IDH1* mutation status was confirmed in all cell lines (Figure S1B). To further support the investigation of ZTR in IDH-mutant gliomas, we examined six primary patient-derived GSC with *IDH1* mutation in sequential quantitative high-throughput screen (HTS) of 2,481 FDA-approved and investigational drugs. This HTS has been applied to various cancer research, including brain tumors.[12,13] A Central Nervous System Multiparameter Optimization (CNS MPO) Score has been developed and utilized to estimate the ability of BBB penetration of the drug and prioritize drugs for CNS disease.[14,15] ZTR was found to be one of few drugs showing both a high efficacy for cell death and the capacity to penetrate BBB (MPO >4 and area under the curve (AUC) *Z* score<−3), indicating ZTR is one of the most effective agents among all screened compounds that can be used in patients treating IDH-mutant gliomas (Figure 1D).

ZTR confers survival benefit in *in vivo* models of IDH-mutant gliomas

Following the observation of superior efficacy in IDH-mutant cells, *in vivo* experiments were conducted to examine the survival benefit of ZTR treatment. ATP-binding cassette (ABC) transporter proteins, including P-glycoprotein transporters (Pgp, encoded by *ABCB1*), multidrug resistance-associated protein (MRP1, encoded by *ABCC1*), and ABC family member G2 (encoded by *ABCG2*) are known to transport a wide range of chemotherapies and targeted drugs, leading to cancer drug resistance.[16] To determine whether ZTR is a potential substrate of ABC transporter proteins, we tested the treatment response to ZTR in cells overexpressing one of these three major transporter proteins. Cells transfected with *ABCB1* (MDR-19 cells), *ABCG2*(R-5 cells), and *ABCC1* did not show any difference in response to ZTR treatment compared to cells transfected with empty vector pcDNA (Figure S2). However, these cells lines exhibited significant resistance to chemotherapeutic drugs known to be substrates of these transporters, such as mitoxantrone.[17] These findings suggest that ZTR is unlikely to be a substrate for ABC transporters, supporting the BBB penetration. Next, we evaluated the efficacy of ZTR in a syngeneic mouse model bearing orthotopic IDH-wildtype or IDH-mutant gliomas by intracranial implantation of NPA (*shp53/shATRX/wtIDH1*) and NPAI (*shp53/shATRX/mIDH1*^{R132H}) cells, respectively. Seven days after the intracranial tumors were implanted, mice were treated with either vehicle or ZTR (Figure 2A, Study 1). As expected, mice bearing IDH-mutant gliomas survived longer than those with IDH-wildtype tumors. ZTR treatment prolonged survival significantly in an IDH-mutant cohort (30 vs. 33 days, $p = 0.01$) but not in ZTR-treated IDH-wildtype group (18 vs. 20 days, $p = 0.07$) (Figure 2B). While this NPA/NPAI orthotopic mouse model reflect intact immune tumor microenvironment, it is not a patient-derive glioma model. We further examined the survival benefit of ZTR in a patient-derived xenograft murine glioma model (Figure 2A, Study 2) established by intracranial injection of isogenic GBM1-wildtype (65 vs. 62 days, $p = 0.73$) or GBM1-mutant (69 vs. 76 days, $p = 0.03$) cells (Figure 2C). In both *in vitro* mouse glioma models, a statistically significant prolonged survival was observed in IDH-mutant but not wildtype models. To examine the drug effect in tumor tissue, pharmacodynamic markers were evaluated utilizing the tumor samples collected from the mice treated with vehicle or ZTR. CDK9 phosphorylation was found to be suppressed in tumors from ZTR-treated mice compared to the DSMO-treated ones in the NPAI (IDH-mutant) group but not in the NPA (IDH-wildtype) mice. The expression of γ-H2A.X, an indicator of DNA damage, was observed in both IDH-wildtype and IDH-mutant groups following

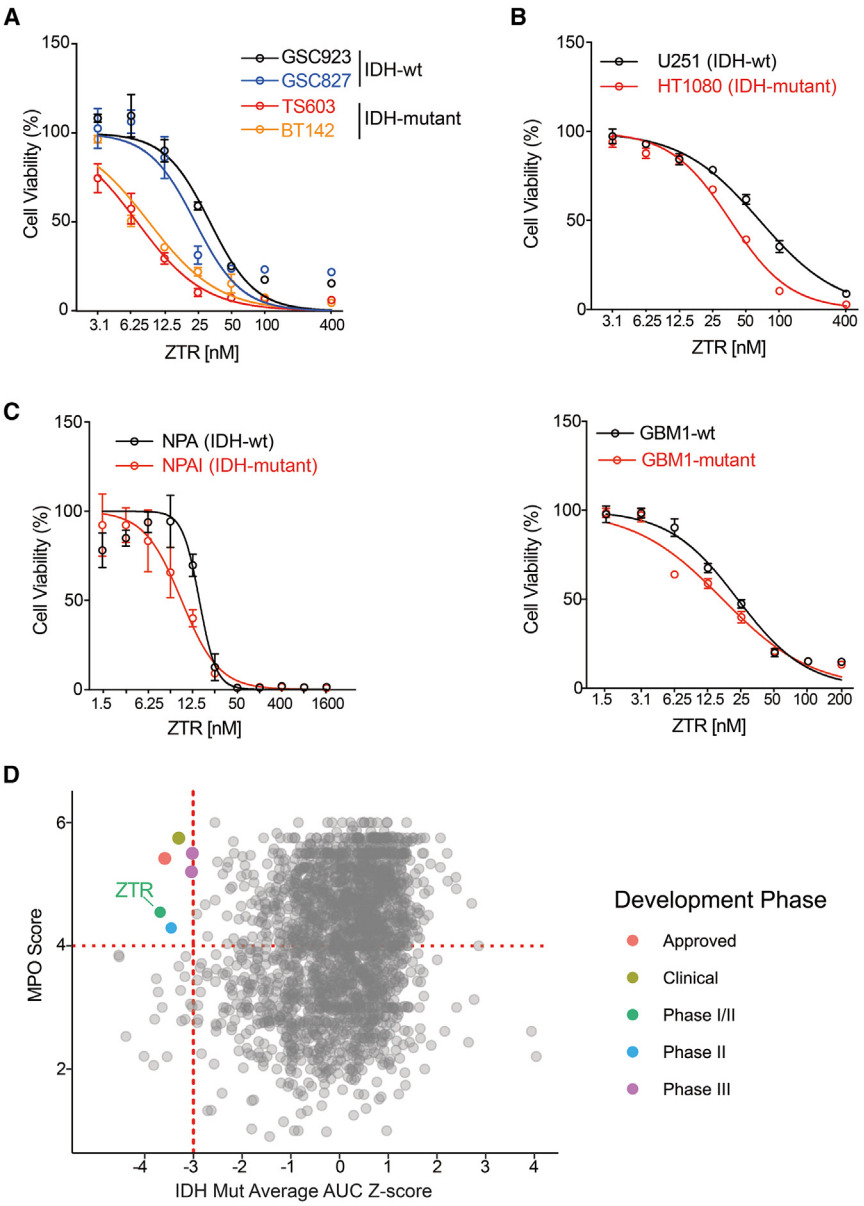

Figure 1. ZTR exhibits enhanced anti-glioma effects on IDH-mutant glioma cells

(A–C) The cytotoxic effect of ZTR in A. patient-derived stem-like glioma cells that are cultivated in 3D environment. GSC923 and GSC827 were cultured from glioblastoma and habor wildtype IDH. TS603 and BT142 were cultured from IDH-mutant high-grade gliomas; (B) patient-derived adherent tumor cells. U251is IDH-wildtype and HT1080 is a fibrosarcoma cell line with mutant IDH; (C) isogenic mouse-derived cells, NPA (*shp53/shATRX/wtIDH1),* NPAI (*shp53/shATRX/mIDH1*^{R132H}*);* and isogenic human-derived cells. Cells were treated with serial dosages of ZTR for 72 h prior to cell viability assay. For all groups, data are means ± SEM.

(D) A sequential quantitative high throughput drug screen of 2,481 FDA-approved or investigational drugs utilizing six primary patient-derived glioma cell lines with *IDH1* mutations was performed. MPO score against average AUC *Z* Score of these primary patient-derived glioma cell lines with *IDH1* mutations showing that ZTR (green dot) was one of the few agents having both high efficacy and capacity to penetrate BBB, defined as AUC *Z* score < −3 and MPO >4, respectively. MPO: CNS Multiparameter Optimization Score.

treatment but was more significant in the IDH-mutant group (Figure 2D). The findings of CDK9 activity suppression and DNA damage induction in tumor tissues from treated mice further support the BBB penetration of the drug and identified potential pharmacodynamic biomarkers of ZTR treatment for clinical investigation. To further validate the selective sensitivity to ZTR treatment in IDH-mutant tumors, we employed a 3D microtumor model that contains an intact tumor microenvironment,[18–20] utilizing fresh tumor obtained from surgery, focusing on the drug effects specific to gliomas, including both IDH-mutant and wild-type (Figure 2E). Five human primary CNS tumor samples including 3 IDH-mutant and 2 IDH-wildtype, were processed and tested against ZTR with the same dosing schedule. An overall decrease in tissue viability was observed in all three IDH-mutant gliomas, but not in the IDH-wild-type samples, indicating the vulnerability of IDH-mutant gliomas to ZTR (Figure 2E, Table S1).

LD ZTR induces higher level of transcriptomic change in IDH-mutant cells

To investigate the selective sensitivity of IDH-mutant vs. IDH-wildtype cells to ZTR, we selected a lower dose (LD) of ZTR (15 nM) in contrast to 50 nM, which was used to treat patient-derived glioblastoma cells in our previous *in vitro* studies. Live-cell imaging analysis by IncuCyte revealed an enhanced suppression of cell proliferation in IDH-mutant cell lines (TS603 and BT142) following LD ZTR treatment, while no significant effect was observed in IDH-wildtype cells (GSC923 and GSC827) (Figure 3A). The proliferation data showed a significant difference from control after 42 h in TS603 and 12 h in BT142. To explore the critical gene and pathway alterations induced by the LD ZTR, we performed RNA sequencing (RNAseq). Pathway analysis with Gene Ontology (GO) demonstrated several cell cycle related pathways downregulated in ZTR-treated TS603 cells after 24 h of treatment (Figure 3B). Moreover, the suppression of cell cycle-related pathways was maintained 48 h after ZTR treatment (Figure S3A). On the other hand, several pathways were identified to be upregulated in the ZTR-treated TS603 cells, including ribosome biogenesis, mRNA processing and macroautophagy. These suggest the possibility of an adaptive response to cell

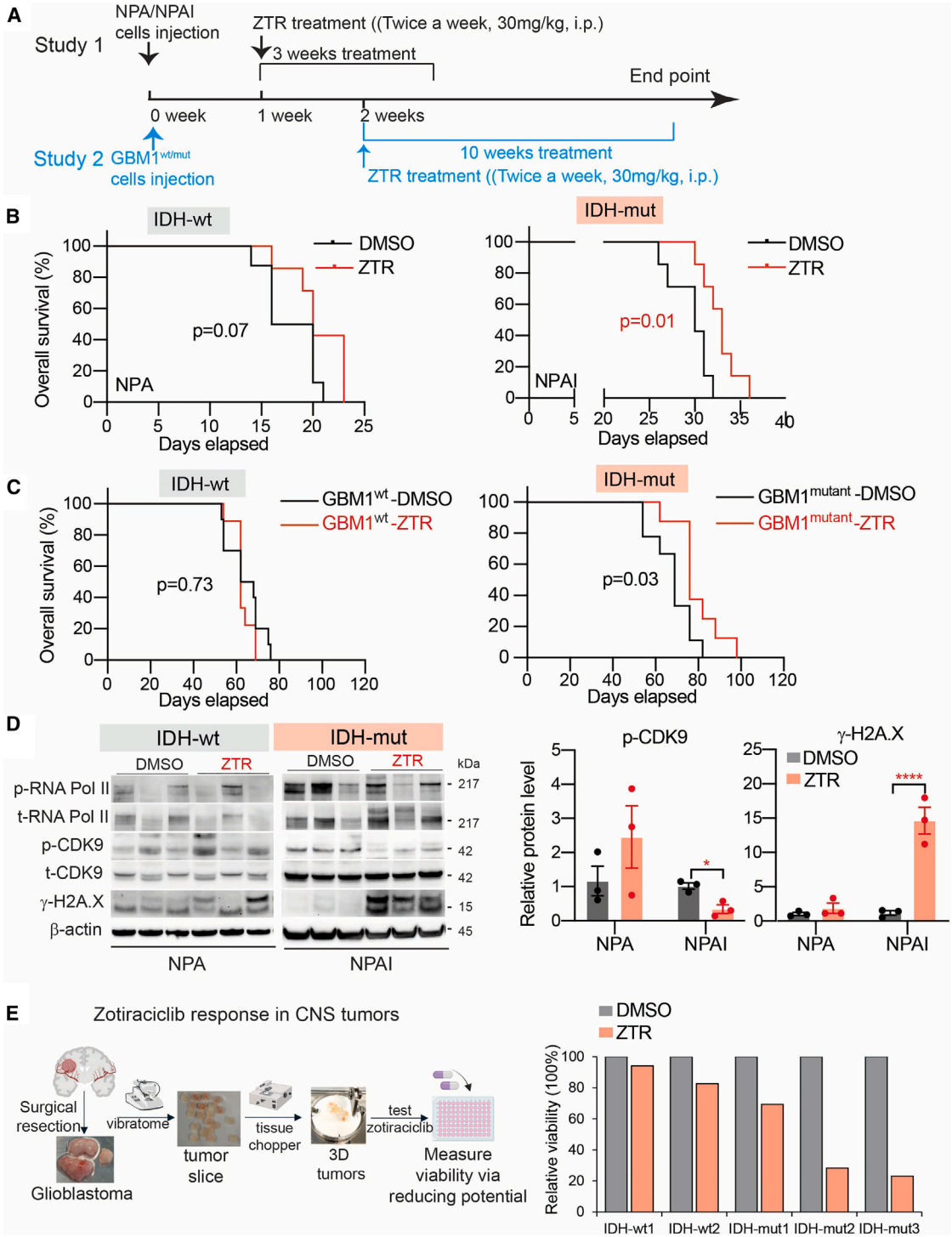

Figure 2. ZTR confers survival benefit in *in vivo* models of IDH-mutant gliomas and glioma patient

(A) Schematic illustration for experimental 1, treating tumor-bearing mice with intracranial IDH-mutant (NPAI, *shp53/shATRX/mIDH1*^{R132H}) or IDH-wildtype (NPA, *shp53/shATRX/wtIDH1*); and experimental 2, patient-derived xenograft mouse model with intracranial GBM1^{IDHmut} or GBM1^{IDHwt} and the ZTR dosing schedule.

(B) Kaplan-Meier analysis of syngeneic allograft glioma mouse model by orthotopically implanting NPA/NPAI cells following ZTR treatment.

(C) Kaplan-Meier analysis of patient-derived xenograft mouse glioma model by orthotopically implanting GBM1-wildtype/-mut cells following ZTR treatment.

(legend continued on next page)

proliferation/cell cycle suppression. Differential expression analysis revealed a higher number of differentially expressed genes (DEGs) in TS603 compared to GSC923 upon LD ZTR treatment for 24 and 48 h, indicating an elevated level of transcriptomic change by LD ZTR treatment in IDH-mutant glioma (Figure 3C). The divergence in its effect on the transcriptome in these two groups partially explained by the selective vulnerability to LD ZTR treatment in IDH-mutant cells. This argument is further supported by the observation of a large number of DEGs in IDH-wildtype glioma when higher dose of ZTR (50 nM) was administered (Figure S3B).

ZTR suppresses mitochondrial complexes and induces mito-stress in IDH-mutant glioma cells

Mutant IDH is known to induce altered cell metabolism and increase dependence on oxidative mitochondrial metabolism.[21,22] Previously, we demonstrated that ZTR induces mitochondria dysfunction in glioblastoma cells at 50nM.[23] To investigate ZTR-induced mitochondrial changes in IDH-mutant glioma, we first examined the cellular organelle morphological changes induced by LD ZTR using a transmission electron microscopy (TEM) examination in GSC923 and TS603 cells. In LD ZTR-treated IDH-mutant TS603 cells, mitochondria appeared dysmorphic and decreased in size. There was an increased number of double-membraned vesicles, varying in size and filled with digested materials, suggesting autophagy (Figure 4A). We then focused on mitochondria and conducted an experiment using Mito Tracker Green Fluorescence Microscope (FM) labeling. The results showed a significant loss of mitochondrial mass in the IDH-mutant glioma cells after LD ZTR treatment but not in the IDH-wildtype glioma cells (Figures 4B and 4C). Next, we examined the impact of LD ZTR on mitochondrial respiration complexes. The expression of genes encoding Complexes I–V and other pathway activity signature genes (Table S2) was suppressed by LD ZTR specifically in TS603 cells, but not in GSC923 cells (Figure 4D). This expression profile was also confirmed by the quantitative expression assay on pathway-focused genes encoding mitochondrial complexes using a profiler PCR array (Figure S4). Protein expression of most complexes was decreased in IDH-mutant cells (TS603 and BT142) following LD ZTR treatment, as observed in native blue gel of the mitochondrial pellet (Figure 4E). To further confirm the suppression of complex activity, an in-gel activity assay for Complex I was performed, revealing ZTR-induced activity suppression only in IDH-mutant TS603 and BT142 cells, but not in IDH-wildtype GSC923 and GSC827 cells (Figure 4F). Although there was a decrease in protein expression level after LD ZTR in GSC827 (Figure 4E), a decrease in its activity wasn't detected (Figure 4F). The suppressed activity of complexes led to a significant reduction in the oxygen consumption rate (OCR) in IDH-mutant cells, indicating decreased oxidative phosphorylation and increased oxidative stress. Surprisingly, the extracellular acidification rate (ECAR), which is expected to increase in stress responses, was reduced in IDH-mutant cells[24] (Figure 4G). Importantly, ATP production through mitochondrial respiration and glycolysis was significantly decreased in the IDH-mutant cells, suggesting a severe bioenergetic failure after LD ZTR treatment (Figures 4H and 4I).

ZTR-induced mito-stress intensifies the imbalance of redox pathway in IDH-mutant glioma cells

Complex I is essential for regenerating NAD in the mitochondria.[25] The deficiency in Complex I induced by ZTR may further interrupt the NAD/NADH balance. In our IDH-mutant cell model, we observed a lower baseline level of NAD expression compared to the IDH-wildtype cell (Figures 5A and S5), which is consistent with the previously reported findings.[26] While ZTR-induced NAD suppression was observed in both IDH-mutant and IDH-wildtype cells, the NAD levels reduction was much more pronounced in IDH-mutant gliomas upon LD ZTR treatment (Figure 5A). Nicotinamide phosphoribosyltransferase (NAMPT) and nicotinate phosphoribosyltransferase domain containing 1 (NAPRT1) are two major rate-limiting enzymes involved in NAD synthesis that determine NAD levels.[27] The NAMPT activity assay failed to show a ZTR-induced NAMPT activity suppression up to a concentration of 50 nM, while a positive control, FK866, significantly reduced NAMPT activity (Figure 5B). Protein expression of NAMPT and NAPRT1 was not affected by LD ZTR treatment, suggesting that the reduction in NAD induced by ZTR is unlikely due to the suppression of NAMPT and NAPRT1. However, we observed a significant reduction in expression of poly (ADP-ribose) glycohydrolase (PARG) following LD ZTR in IDH-mutant glioma cells (Figure 5C). PARG is an enzyme involved in degrading ADP-ribose polymers to release NAD for re-use. The mechanism underlying the reduction in PARG is unclear, but it may contribute to the further reduction in NAD levels. In summary, LD ZTR reduced NAD levels in IDH-mutant glioma cells through the suppression of Complex I and PARG expression. The impact of ZTR-induced NAD reduction was expected to be greater in IDH-mutant gliomas, which inherently have lower levels of NAD compared to their IDH-wildtype counterpart.

Oxidative stress induces the production of mitochondrial reactive oxygen species (ROS), disrupting redox homeostasis.[28] LD ZTR significantly increased ROS production in the IDH-mutant cells, indicating mito-stress is induced after LD ZTR treatment (Figure 5D). To counterbalance the excessive ROS, a substantial amount of antioxidant is consumed, as evidenced by a significant decrease in GSH/GSSG ratio in IDH-mutant cells (Figure 5E). NADPH, which is critical for glutathione and thioredoxin systems to neutralize ROS, is largely consumed by 2-HG production in IDH-mutant cells,[29] consistent with the lower baseline level of NADPH/NADP ratio in IDH-mutant cells demonstrated in Figure S5. In addition, LD ZTR treatment further reduced NADPH/NADP ratio to a greater extent in IDH-mutant cells

(D) Left: Western blotting showing protein expressions of CDK9, and RNA Pol II phosphorylation and γ-H2A.X in tumor tissues from mice from control or ZTR treatment cohort. β-actin was blotted as internal control. Right: Statistic analysis of *p*-CDK9 and γ-H2A.X relative protein levels, which was normalized to β -actin. For all groups, data are mean ± SD. Statistical analysis were performed by two-way ANOVA combind with unpaired t-test. *, $p < 0.05$; ***, $p < 0.001$.
(E) Zotiraciclib response in *ex vivo* tumor tissue. Left: Illustration showing preparation and treatment response evaluation in 3D micro (μ) tumor using fresh patient tumor samples. Right: Relative viability of the tumors from IDH-wildtype ($n = 2$) and IDH-mutant primary CNS tumors ($n = 3$) in response to ZTR treatment.

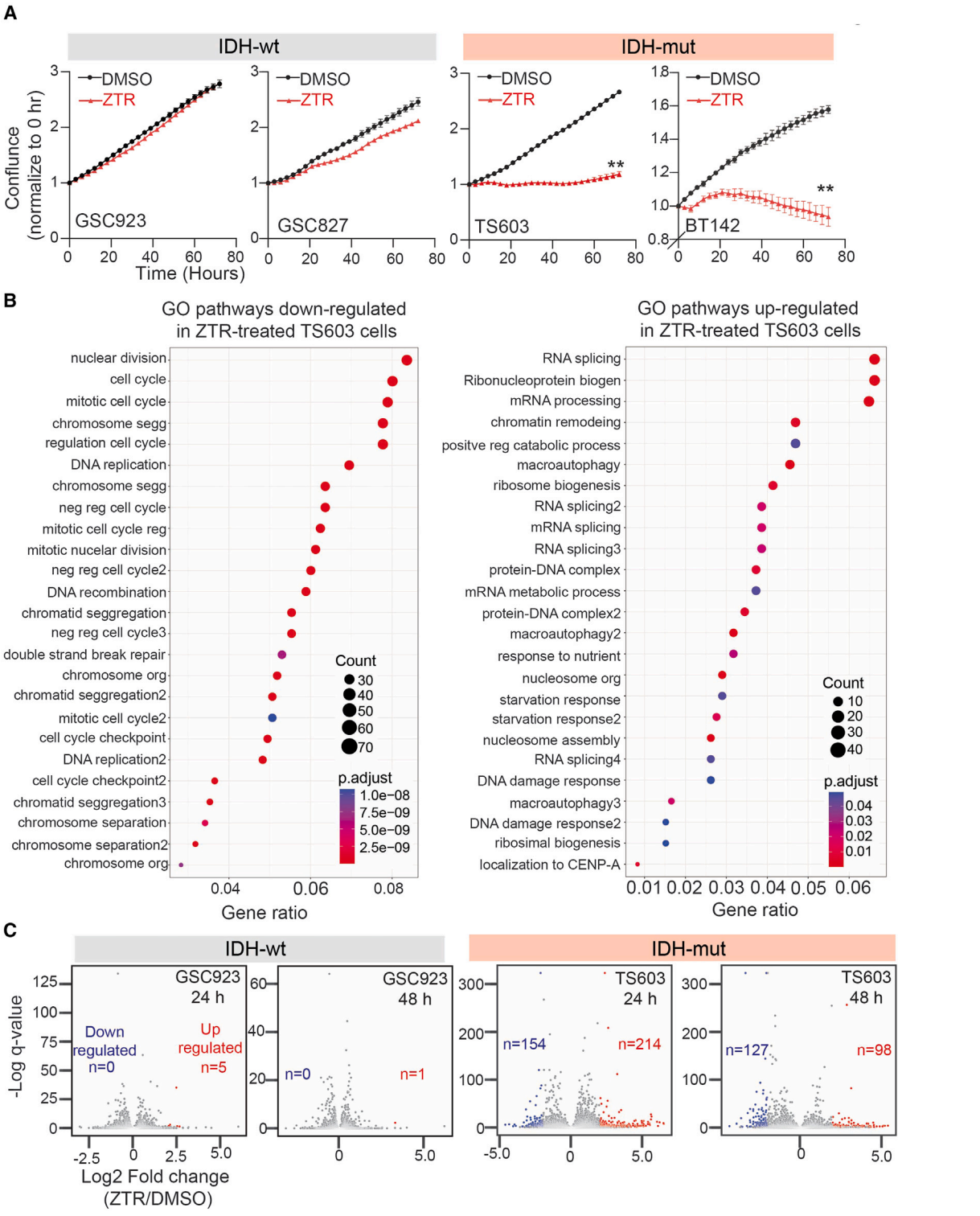

(legend on next page)

compared to IDH-wildtype cells (Figure 5F). In patient derived IDH-mutant GSCs, the NADPH/NADP ratio was downregulated by 30.3% and 40.5% in TS603 and BT142, respectively. However, there was only an 11.3% decrease in the IDH-wildtype GSC827 and no change in IDH-wildtype GSC923 (Figure 5F). The crucial enzymes G6PD and PGD, responsible for NADPH production, were not altered after ZTR treatment (Figure 5C). Collectively, these results suggest that the low NADPH is likely caused by the increased consumption rather than decreased production of NADPH, thereby exacerbating the ROS imbalance in IDH-mutant gliomas.

As a cellular self-defense mechanism in response to increased ROS production, a group of genes encoding antioxidants is expected to be activated to eliminate excessive ROS. However, the activity of antioxidant response element (ARE) luciferase, which reflects transcriptional activation of those genes, was found to be decreased rather than increased in IDH-mutant cells (Figure 5G). The mechanisms underlying this paradoxical reduction in ARE luciferase activity are unclear, but it further contributes to the redox imbalance. Excessive ROS production is a well-recognized mediator of induced DNA damage. In IDH-mutant cells, more genomic DNA fragmentation was observed compared to IDH-wildtype cells (Figure 5H). We further analyzed the enrichment of signaling pathways based on the RNA-seq data from TS603. KEGG pathway enrichment analysis showed ZTR-induced suppression in multiple DNA damage repair (DDR) pathways and thereby increase DNA damage and cell death (Figure 5I).

LD ZTR induces cell death in IDH-mutant glioma cells

We previously demonstrated the suppression of RNA Pol II and CDK9 activity in glioblastoma cells treated with ZTR at a concentration of 50 nM.[11] In this study, we observed a similar suppression in IDH-mutant, but not IDH-wildtype glioma cells, when treated with LD ZTR at 15 nM (Figure 6A). The expression of short-lived anti-apoptotic proteins, namely MCL-1, XIAP and survivin, were also suppressed by LD ZTR in IDH-mutant cells (Figure 6B-a). Activation on c-PARP and γ-H2A.X further indicates the induction of DNA damage by LD ZTR in IDH-mutant cells, but not in IDH-wildtype cells (Figure 6B-b). Caspase 3/7 activity, a biomarker of apoptosis, was significantly increased in IDH-mutant cells following LD ZTR treatment, while no significant change was observed in IDH-wildtype cells (Figure 6C). The activation of caspase 8 and caspase 9 suggested that both intrinsic and extrinsic apoptosis pathways may have been activated as early as 6–12 h in LD ZTR-treated IDH-mutant cells (Figure 6D). Apoptosis was further analyzed by flow cytometry, which showed an increase in the percentage of both early and late apoptotic cells in LD ZTR-treated IDH-mutant cells, but not in IDH-wildtype cells (Figure 6Ea). Interestingly, a pan-apoptosis inhibitor, Z-VAD, only partially rescued the cell death (Figure 6Eb). These results suggest that apoptosis, a programmed ATP-dependent cell death, may not be major type of cell death in ZTR-treated cells. The cellular organelle morphological changes after the LD ZTR treatment suggested that autophagy may have been induced (Figure 4A). In addition, the RNA-seq analysis in LD ZTR-treated cells indicated the upregulated autophagy pathway (Figure 3C). LD ZTR treatment-induced cleavage of LC3B, an autophagy marker was demonstrated in IDH-mutant glioma cells (Figure S6A). Overall, multiple cell death mechanisms may be involved in LD ZTR-induced cell death in IDH-mutant cells.

PIM is identified as a target of ZTR in glioma

To elucidate the specific signaling pathways that may be involved in ZTR-mediated bioenergetic failure, we analyzed gene expression changes in TS603 cells treated with ZTR for 24 h (Figure 7A). Pathway enrichment analysis was performed on 915 significantly downregulated genes by ZTR, with at least a 2-fold decrease in expression. We identified an enrichment of genes related to Mitochondrial Complex I assembly, with a *p*-value of 0.04. Subsequently, we utilized the ZTR-downregulated genes associated with mitochondrial complex assembly to infer potential upstream kinases[30] that might regulate these genes. Utilizing the eXpression2Kinases (X2K) method for kinase enrichment analysis identified the Provirus Integration site for Moloney leukemia virus (PIM) family of kinases as potential candidates capable of regulating ZTR-induced mitochondrial dysfunction. To validate this hypothesis, we performed kinase activity assays to determine whether ZTR directly inhibits PIM kinases. Interestingly, we found that ZTR is a potent inhibitor not only of several CDK kinases, JAK2, and FLT3, as reported previously,[8] but it also effectively inhibits PIM1 and PIM3 kinases (Figure 7B). Consistently, phosphorylation of PIM1/3 was notably reduced following LD ZTR treatment in IDH-mutant glioma cells but not in IDH-wildtype ones. These results imply that LD ZTR exerts a greater inhibitory influence on PIM1/3 activity specifically in IDH-mutant cells (Figure 7C). To explore whether the biological effects of LD ZTR can be induced by a direct inhibition of PIM1/3 inhibition in glioma cells, we performed the live-cell imaging analysis by IncuCyte following the treatment with AZD1208, a pan-PIM inhibitor. Direct PIM inhibition induced a significant suppression of cell proliferation in IDH-mutant cell lines (TS603 and BT142), but not in IDH-wildtype cells (Figure 7D). Treatment with PIM inhibitor induced a significant reduction in ATP production, specifically in ATP generated from oxidative phosphorylation, in IDH-mutant cells rather than IDH-wildtype cells (Figure 7E). The effects of the PIM inhibitor on cell proliferation and

Figure 3. LD ZTR suppresses cell proliferation and induces higher level of transcriptomic change in IDH-mutant glioma cells

(A) Cell proliferation assay of primary patient-derived stem-like cells, IDH-wildtype (GSC923 and GSC827) and IDH-mutant (TS603 and BT142) following 15 nM ZTR treatment. All cells were maintained and treated in 3D culture. Phase area confluence was measured every 3 h by IncuCyte up to 72 h. All cell line data were normalized to its own start time point (0 h) value. For all groups, data are means ± SEM. Unpaired t-test was performed for comparisons of two groups at 72 h. **, $p < 0.01$.

(B) Enriched Gene Ontology (GO) pathways downregulated (left) or upregulated (right) in TG603 cells in response to ZTR treatment at 15 nM for 24 h.

(C) Volcano plots based on RNA-seq results showing the number of differentially expressed genes after ZTR treatment at 15 nM for 24 or 48 h in IDH-wildtype (GSC923) and IDH-mutant (TS603) cells $n = 3$. **, $p < 0.01$, Two-sample t-test at each time point with the Bonferroni correction.

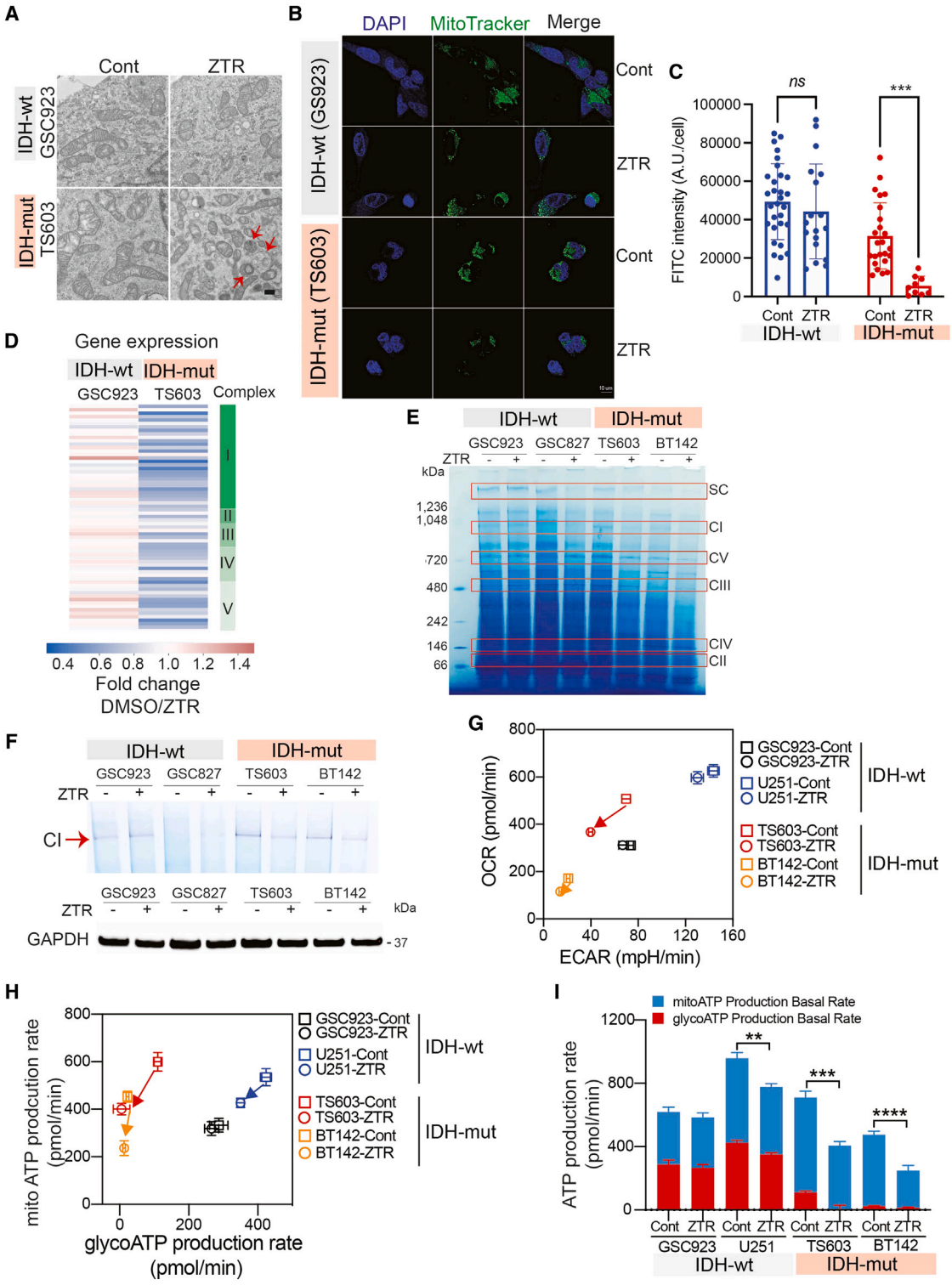

Figure 4. LD ZTR treatment suppresses mitochondrial complexes and induces biogenic energy depletion in IDH-mutant glioma cells

(A) Transmission electron microscope pictures showing the mitochondrial morphology changes and the presence of double-membraned vesicles, filled with digested materials (indicated by red arrows), consistent with autophagy in TS603 cells after ZTR treatment at 15 nM for 48 h. Scale bar = 500 nm.

(B) MitoTracker Green FM staining demonstrating the mitochondrial mass volume change after ZTR treatment at 15 nM for 48 h in IDH-wildtype and IDH-mutant cells. Scale bar = 10 μm.

(legend continued on next page)

ATP reduction are consistent with those caused by LD ZTR treatment (Figures 3A and 4I). Along with the biochemical assay results (Figure 7B), these findings suggest that the unexpected inhibition PIM kinase could contribute to the inhibitory action of LD ZTR. Notably, PIM kinases were reported to be constitutively active when expressed in cells and their activity is correlated with the expression level.[31] Consequently, the higher protein expression levels of PIM1/3 in IDH-mutant cells compared to IDH-wildtype cells (Figure 7F) indicate elevated PIM activity in the mutant cells. To examine the PIM kinase activity in independent datasets, we adopted a systems-based approach to determine whether PIM kinase-associated gene signature is enriched in IDH-mutant gliomas. We first identified mitochondrial metabolic pathway genes that are downregulated in response to ZTR treatment, which are known to be driven by PIM kinases (using Genes2Networks: http://actin.pharm.mssm.edu/genes2networks[32]). We then investigated whether these PIM-driven mitochondrial pathway genes were enriched in IDH-mutant gliomas. Our analysis of 66 patient glioma samples (IDH-mut, n = 44, IDH-wildtype, n = 22) indicated that PIM-associated mitochondrial genes are significantly enriched in IDH-mutant tumors compared to wild-type (Figure S7). This enrichment supports the increased PIM kinase activity in IDH-mutant gliomas and could explain why IDH-mutant tumors exhibit aberrant mitochondrial activity in response to ZTR treatment. Finally, we examined the protein expression of PIM1 in a group of patient glioma samples (IDH-mutant, n = 3; IDH-wildtype, n = 3) by immunohistochemical staining. Overall, an increased PIM1 expression is observed in IDH-mutant gliomas compared to IDH-wildtype gliomas (Figure 7G). In conclusion, as depicted in Figure 7H, our findings suggest that ZTR's impact on mitochondrial Complex I assembly and bioenergetic failure in IDH-mutant cells may be mediated, in part, by its potent and unexpected inhibition of PIM1 and PIM3 kinases.

DISCUSSION

In this study, we demonstrated a selective sensitivity to ZTR across multiple *in vitro* IDH-mutant gliomas models cultivated in 3D environment and *ex vivo* models utilizing patients' fresh tumor samples. A survival benefit was demonstrated in both syngeneic and PDX mouse models with orthotopic IDH-mutant gliomas. Notably, we showcased a durable response to ZTR treatment in a patient with recurrent IDH-mutant astrocytoma. To support further clinical investigation of ZTR in IDH-mutant glioma patients, we identified that ZTR is one of the few drug candidates among a panel of 2,481 FDA-approved or investigational drugs, exhibiting selective sensitivity in IDH-mutant glioma while penetrating BBB in a high throughput drug screen. Mechanistically, we revealed that LD ZTR specifically suppressed mitochondrial complex activities in IDH-mutant gliomas, leading to a decreased NAD level, impaired ATP production, and thereby inducing mito-stress. Notably, we identified PIM kinases as a new target of ZTR, linking the ZTR-induced bioenergetic failure and cell growth suppression with PIM inhibition in glioma. The inherent redox imbalance of IDH-mutant gliomas and the compromised ROS clearance capability further contributed to the accumulation of ROS upon ZTR treatment. Increased ROS and suppressed DDR led to enhanced DNA damage. Furthermore, ZTR suppressed the CDK9/RNA PO-LII phosphorylation pathway, resulting in decreased expression of antiapoptotic proteins and contribute to cell death. In summary, as illustrated in graphic abstract, ZTR induced bioenergetic failure, DNA damage, and apoptosis, ultimately leading to the death of IDH-mutant glioma cells.

Connecting ZTR-induced mitochondrial dysfunction with PIM kinases

PIM kinases belong to the family of serine/threonine protein kinases. Three isoforms- PIM1, PIM2 and PIM3 have been identified, with PIM 1 and 2 sharing very similar kinase domains.[33] All three isoforms are constitutively active, phosphorylate serine/threonine amino acids and activate similar cellular pathways.[34,35] PIM kinases have a wide range of phosphorylation targets involved in multiple signaling pathways, playing significant roles in tumorigenesis and tumor progression in both solid and hematologic cancers.[35,36] Importantly, PIM inhibition has been reported to cause mitochondrial fragmentation and increased intracellular ROS in lung cancer.[37] Utilizing an integrated biochemical profiling of ZTR targets and transcriptomic analysis, we identified PIM as a new target of ZTR in addition to what was reported previously, linking the ZTR-induced cell proliferation suppression and mitochondrial dysfunction in gliomas with PIM inhibition. We not only provided evidence of enhanced expression of PIM1/3 in our glioma cell line models and patients' tumor tissue, but also validate the enrichment of PIM-associated mitochondrial genes in IDH-mutant gliomas in a larger database published previously.[38] Collectively, these findings provide a profound mechanistic understanding of why LD ZTR triggers mitochondrial dysfunction in IDH-mutant gliomas.

The inherent metabolic features of IDH-mutant glioma contribute to their therapeutic vulnerability to ZTR

The increased sensitivity to ZTR in IDH-mutant glioma is believed to stem from the biological vulnerability of these tumors, which

(C) Mitochondrial mass was calculated as the MitoTracker Green FM positive area per cell in 2D cross-sectional images using ImageJ software. For all groups, data are mean ± SD. Statistical analysis were performed by two-way ANOVA test. ***, $p < 0.001$.
(D) Cells were cultured and treated in 3D culture. RNAseq results showing absolute fold change in expression level of the signature genes coding for mitochondrial complexes after ZTR treatment at 15 nM for 48 h, in GSC923 and TS603 cells.
(E) Cells were cultured and treated in 3D culture. Native blue gel staining of mitochondrial complexes protein after ZTR treatment at 15 nM for 48 h in IDH-wildtype (GSC923 and GSC827) and IDH-mutant (TS603 and BT142) cells.
(F) In-gel activity assay showing the Complex I activity changes after ZTR treatment at 15 nM for 48 h. GAPDH was blotted as internal control.
(G) Mito-stress seahorse assay showing mitochondrial stress by measuring the OCR and ECAR after ZTR treatment at 15 nM for 24 h.
(H and I) Real-time ATP seahorse assay measuring mitoATP and glycolATP production changes after ZTR treatment at 15 nM for 24 h. For all groups, data are means ± SEM. Unpaired t-test was performed for comparisons of two groups. **, $p < 0.01$; ***, $p < 0.001$; ****, $p < 0.0001$.

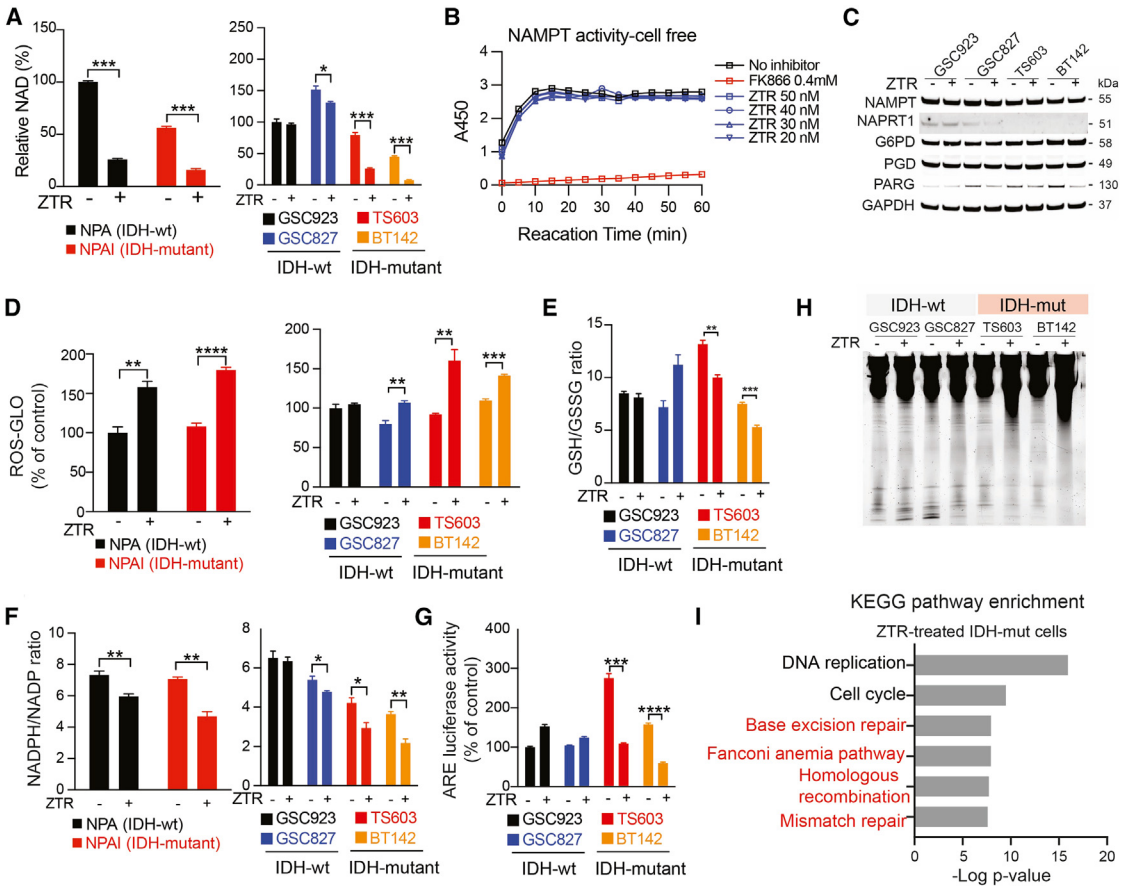

Figure 5. LD ZTR-induced mito stress intensifies the imbalance of redox pathway in IDH-mutant glioma cells

(A) NAD-Glo assay measuring NAD level changes in NPA/NPAI or GSC cells after 48 h treatment with ZTR at 50 nM and 15 nM, respectively. The signals were measured after 48 h treatment.

(B) Cell-free NAMPT activity assay measuring NAMPT enzyme activity with different dose of ZTR treatment in time-dependent manner. FK866 was used as a positive control.

(C) Western blotting showing protein levels of NAD and NADPH related enzymes in primary patient-derived stem-like cell lines with and without ZTR treatment at 15 nM for 72 h. GAPDH was blotted as internal control.

(D) ROS-Glo assay measuring the ROS level in NPA/NPAI or GSCs cell lines in 2D culture with and without ZTR for 48 h treatment at 50 nM and 15 nM, respectively.

(E) GSH/GSSG-Glo assay measuring the GSH/GSSG ratio changes in patient-derived GSCs cell lines in 2D culture following ZTR treatment at 15 nM.

(F) NADP/NADPH-Glo assay measuring NADP/NADPH changes in NPA/I or patient-derived GSC cells in 2D culture after ZTR treatment at 50 nM and 15 nM, respectively.

(G) ARE luciferase assay measuring the ARE activity changes in GSCs cell lines in 2D culture with ZTR treatment at 15 nM.

(H) Total genomic DNA electrophoresis analysis showing DNA fragmentation after ZTR treatment at 15 nM for 48 h.

(I) RNAseq results of TS603 cell line showing significantly enriched gene sets related to DNA damage and repair processes after 24 h ZTR treatment at 15 nM. For all groups, data are mean ± SEM. Unpaired t-test was performed for comparisons of two groups. *, $p < 0.05$; **, $p < 0.01$; ***, $p < 0.001$; ****, $p < 0.0001$.

potentiates the effects of ZTR. Specifically, the 2-HG-induced reliance on mitochondrial oxidative phosphorylation for cellular energy production, along with the heightened mitochondrial metabolism in IDH-mutant gliomas,[5,21,39] makes these cells more susceptible to therapies targeting mitochondrial function. In our study, LD ZTR suppressed the expression of respiration complexes at both RNA and protein levels, reduced mitochondria volume in IDH-mutant glioma cells and disrupted oxidative phosphorylation. and ATP production. This disruption contributes to the overall mitochondrial dysfunction observed in these cells.

Additionally, IDH-mutant gliomas exhibit reduced NAD levels, reportedly due to the epigenetic downregulation of NAPRT1, an enzyme involved in NAD+ salvage pathway.[26] In our study, LD ZTR treatment further suppressed NAD+ levels in the IDH-mutant cells. Rather than affecting NAMPT and NAPRT1, the rate-limiting enzymes of the NAD salvage pathway, ZTR was found to suppress the expression of PARG, which is responsible for the degradation of PAR chains and recycling NAD+ back into the system.[40] LD ZTR-induced PARG reduction may further contribute to the shortage of NAD in IDH-mutant glioma cells. Additionally, the mitochondrial Complex I catalyzes the NADH

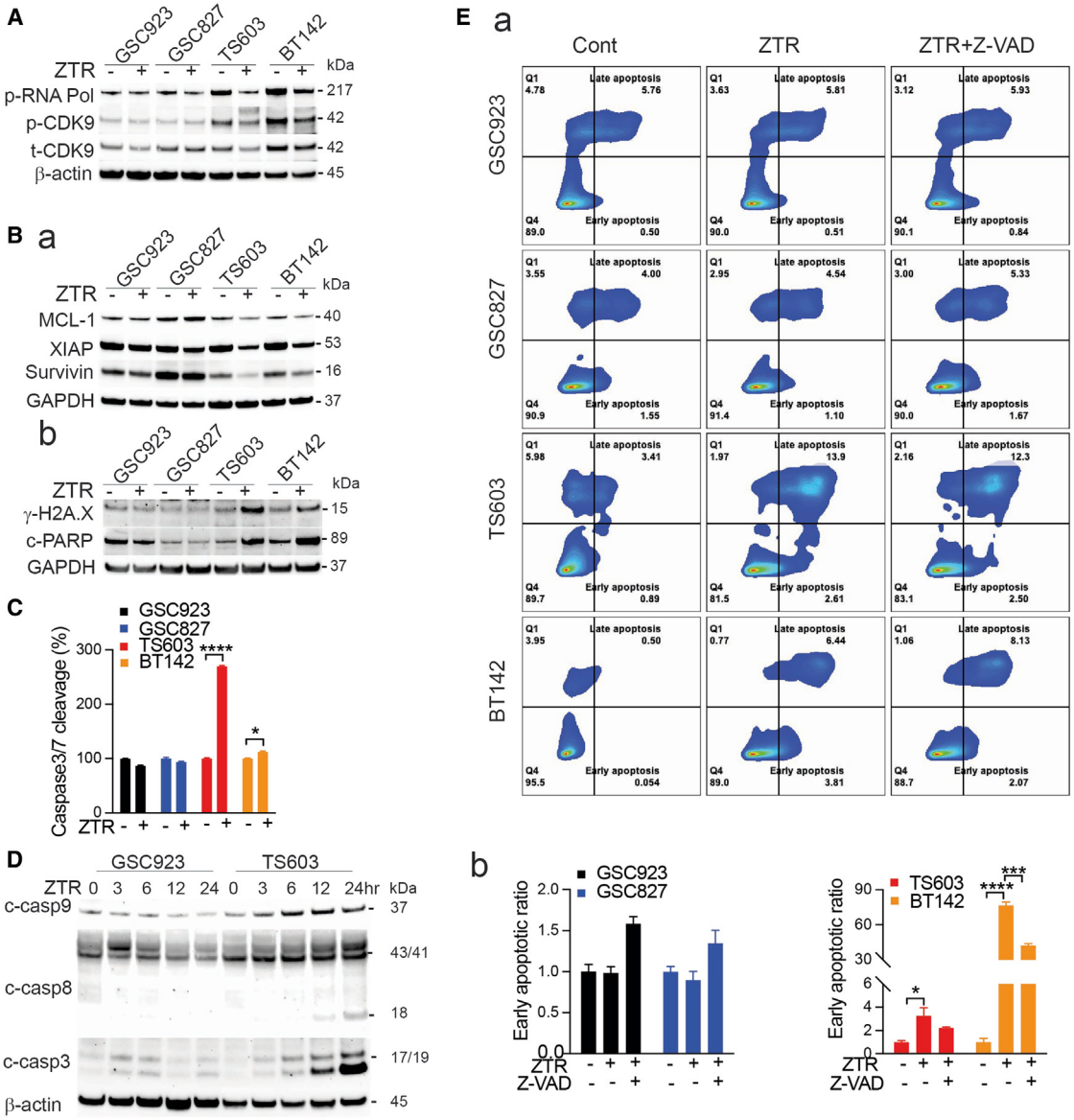

Figure 6. LD ZTR induces DNA damage and cell death in IDH-mutant glioma cells

(A) Western blotting showing CDK9 and RNA Pol II phosphorylation levels with ZTR treatment at 15 nM for 72 h. β-actin was blotted as internal control.

(B) (a) Western blotting showing expression levels of MCL-1, XIAP, and survivin, short-lived antiapoptotic proteins, following ZTR treatment at 15 nM for 48 h. (b) Western blotting showing protein expression levels of γH2AX and cleaved (c)-PARP with ZTR treatment at 15 nM for 72 h. GAPDH was blotted as internal control.

(C) Caspase 3/7-Glo assay showing caspase 3/7 activity changes after ZTR treatment at 15 nM for 72 h in primary patient-derived GSCs.

(D) Western blotting showing cleavage of caspase 9, 8 and 3 after ZTR treatment at 15 nM in GSC923 (IDH-wildtype) and TS603 (IDH-mutant). Samples were collected at 0, 3, 6, 12, and 24-h after treatment. β-actin was blotted as internal control.

(E) (a) Flow cytometry assay measuring the percentage of early/late apoptotic and necrotic cell by staining with APC Annexin V/PI after 15 nM ZTR alone or both 15 nM ZTR and 10 μM Z-VAD for 72 h. DMSO treatment was used as a control. (b) Statistic analysis of early apoptotic ratio in all cell lines tested. For all groups, data are means± SEM. Unpaired t-test was performed for comparisons of two groups. *, $p < 0.05$; **, $p < 0.01$; ***, $p < 0.001$; ****, $p < 0.0001$.

oxidation and the elevation of NAD+, which is essential for energy production. The suppression of Complex I activity by the LD ZTR treatment may partially contribute to the reduction of NAD induced by ZTR.

Furthermore, NADPH plays a critical role in clearing accumulated ROS and relieving oxidative stress.[41] In IDH-mutant glioma cells, the conversion of α-KG to 2-HG excessively consumes NADPH, resulting in an imbalance of redox homeostasis.[42,43] LD ZTR treatment, by suppressing respiration complexes, particularly Complex I, further increases ROS production and exacerbates the pre-existing redox imbalance. This results in a more pronounced impact on IDH-mutant glioma cells, making them more susceptible to the ZTR treatment.

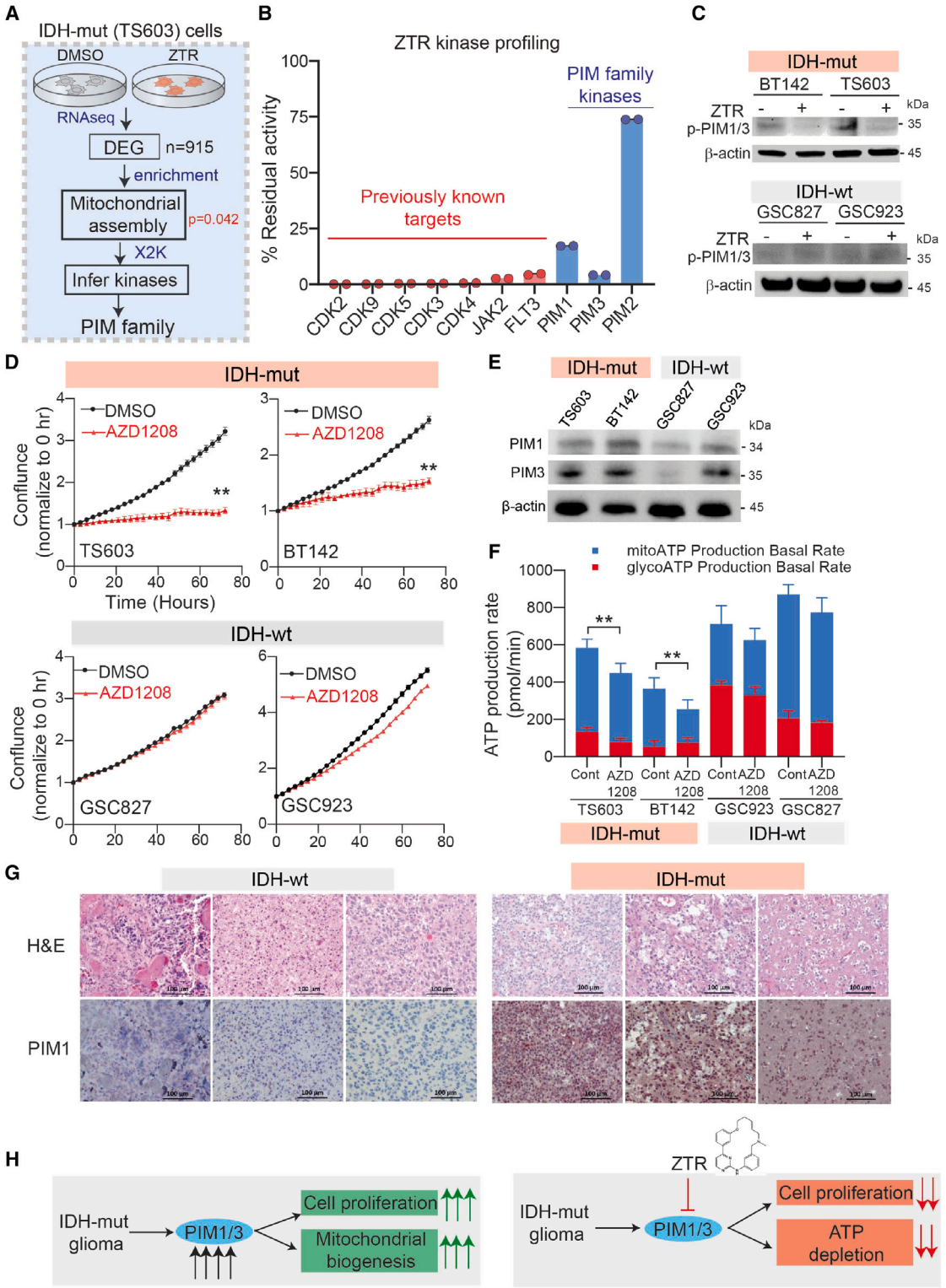

Figure 7. PIM1/3 are targets of ZTR, mediating enhanced effects in IDH-mutant gliomas

(A) Schematically illustrating an integrated pathway enrichment and upstream kinase inference approach that were utilized to identify PIM kinases as potential targets of ZTR associated with mediating mitochondrial dysfunction.

(B) ZTR (500nM) inhibits the activity of several previously known CDK kinases, and PIM kinases *in vitro*. Bars represent the mean of two independent data points.

(legend continued on next page)

ZTR suppresses stress response pathways in IDH-mutant glioma cells

When cells are under mito-stress, glycolysis is typically upregulated to compensate for the loss of cellular energy.[26] However, in IDH-mutant cells treated with LD ZTR, we observed a suppression of glycolysis rather than enhancement, despite the reduction in oxidative phosphorylation. This suppression in glycolysis may be attributed to the depletion of NAD depletion or the inhibition of glycolytic enzymes by ROS.[40,41] The simultaneous suppression of both oxidative phosphorylation and glycolysis by ZTR resulted in a severe bioenergetic failure in IDH-mutant gliomas.

In response to the increased ROS production, cells typically activate the ROS scavenger systems, such as the GSH/GSSG system and NADPH/NADP to restore redox balance. Additionally, ARE plays a crucial role in mediating the transcriptional activation of genes involved in detoxification and cytoprotection under oxidative stress.[44] However, in our study, despite the presence of increased ROS, LD ZTR treatment failed to activate ARE in IDH-mutant glioma cells. The reasons underlying this suppression are not yet clear, but it suggests a failure to restore redox balance following LD ZTR treatment. Consequently, the excessive accumulation of ROS in IDH-mutant cells may further sensitize them to agents that induce DNA damage, such as ZTR.[45] In addition to the inherent DDR deficiency, LD ZTR-induced depletion of NAD, which serves as the substrate for the PARP signaling pathway, might further contribute to DDR deficiency, particularly in base excision repair, in IDH-mutant cells. Consistently, our study observed the activation of DNA damage markers, γ-H2A.X and cleaved-PARP, and DNA fragmentation in LD ZTR-treated IDH-mutant cells.

The presence of *IDH* mutation in glioma cells has been shown to dynamically reprogram the transcriptome, leading to persistent downregulation of certain transcription factors.[46] Additionally, widespread hypermethylation, particularly in promoter regions and CpG islands close to the transcription start sites, occurs in IDH-mutant cells, resulting in the predominant suppression of gene transcription.[47] Therefore, the aberrant transcriptome of IDH-mutant tumors might further contribute to the vulnerability to ZTR-induced CDK9 and RNA POLII inhibition. We previously demonstrated that treatment with ZTR at a concentration of 50 nM led to a decrease in CDK9 and RNA POLII phosphorylation in IDH-wildtype GSC827 and GSC923 cells. However, when the dosage of ZTR was decreased to 15 nM, this suppression of transcription signaling was only observed in IDH-mutant cells and was no longer detected in IDH-wildtype glioma cells. These findings are consistent with the observation that LD ZTR decreased the expression of short-lived antiapoptotic proteins, MCL-1, XIAP, and survivin in IDH-mutant glioma cells, but not in IDH-wildtype gliomas. Interestingly, while apoptosis and autophagy were observed in the cell death process, the inhibition of these processes alone was not sufficient to completely prevent cell death, indicating the involvement of other cell death mechanisms. While markers of pyroptosis and necroptosis were not detected in ZTR-treated glioma cells (Figure S6B), including those with *IDH* mutations, other cell death mechanisms, such as ferroptosis, warrant further investigation.

Preclinical findings provided rationale for clinical investigation of ZTR in IDH-mutant gliomas

Overall, the preclinical findings in this study have underscored the therapeutic potential of ZTR in targeting IDH-mutant gliomas. We have demonstrated that ZTR disrupts mitochondrial function, particularly through PIM inhibition, suppresses stress response pathways, and induces cell death specifically in IDH-mutant gliomas at a low concentration. The increased vulnerability to the specific mechanisms of action of ZTR has led to the heightened efficacy of the drug treatment in this subset of gliomas with *IDH* mutation. The therapeutic vulnerability to ZTR presents an opportunity to treat IDH-mutant glioma patients with less intense dosing schedule, avoiding the need to combine with other cytotoxic agents, thereby reducing overlapping drug toxicity and improving the patients' quality of life. Building on these promising results, a clinical study (*NCT 05588141*) has been initiated to evaluate the efficacy and safety of ZTR as a monotherapy in IDH-mutant glioma patients. By exploiting the inherent vulnerabilities of IDH-mutant gliomas and leveraging the unique mechanisms of actions of ZTR, this therapeutic approach holds promise for effective tumor control while potentially minimizing treatment toxicities.

Limitations of the study

Our preclinical data indicate that the therapeutic vulnerability to ZTR, presenting an opportunity to treat IDH-mutant glioma patients safely and effectively. However, a key limitation was the modest survival benefit observed in IDH-mutant glioma mouse models, despite the statistically significant prolongation of survival. This modest benefit could be partly due to the more aggressive disease course in the mouse models used, which limits treatment opportunities and does not fully replicate the less aggressive disease course typically seen in human IDH-mutant gliomas compared to their IDH-wildtype counterparts. Human IDH-mutant gliomas often have a longer therapeutic

(C) Western blot showing the activity changes of PIM1/3 following treatment of ZTR in IDH-mutant (BT142 and TS603) and IDH-wildtype glioma cells (GSC923 and GSC827).
(D) AZD1208, a pan-inhibitor of PIM significantly suppresses the cell proliferation in IDH-mutant cells but not in IDH-wildtype cells, demonstrated by the cell proliferation assay using IncuCyte. Phase area confluence was measured every 3 h by IncuCyte up to 72 h. All cell line data were normalized to its own start time point (0 h) value. For all groups, data are means± SEM. Unpaired t-test was performed for comparisons of two groups at 72 h. **, $p < 0.01$.
(E) Western blot showing the increased protein expression of PIM1/3 in IDH-mutant compared to IDH-wildtype glioma cells.
(F) Real-time ATP seahorse assay measuring mitoATP and glycolATP production changes after treatment of AZD1208, a PIM-inhibitor for 24 h. For all groups, data are means ± SEM. Unpaired t-test was performed for comparisons of two groups. **, $p < 0.01$.
(G) immunohistochemical (IHC) staining showing the protein expression of PIM1 in 6 patient glioma samples (IDH-wildtype, $n = 3$; IDH-mutant, $n = 3$). Top panel: tumor sections with H&E stain. Bottom panel: IHC with PIM1 antibody at a dilution of 1:100. The scale bars indicate 100 μm.
(H) A graphic summary to illustrate that ZTR targets PIM1/3 to induce cell proliferation suppression and cellular ATP depletion.

window, potentially allowing for greater survival benefits. To address these limitations, *ex vivo* analysis using patients' tumor samples demonstrated increased sensitivity to ZTR treatment in IDH-mutant gliomas. Given the limited number of the fresh tumor samples from patients, further clinical testing is warranted. A clinical trial aims to further investigate the safety and efficacy of ZTR as a treatment option in IDH-mutant gliomas is ongoing (*NCT 05588141*).

RESOURCE AVAILABILITY

Lead contact

Further information and requests for resources and reagents should be directed to and will be fulfilled by the Lead Contact, Dr. Jing Wu (jing.wu3@nih.gov).

Materials availability

Samples in this study are available from the lead contact upon request, as collaboration, subject to availability.

Data and code availability

- Data: All data supporting the findings of this study are available within the main manuscript and the supplementary files. RNA-sequence data have been deposited at Gene Expression Omnibus and are publicly available as of the date of publication (accession number: GSE252245).
- Code: This paper does not report the original code.
- All other items: Any additional information required to re-analyze the data reported in this paper is available from the lead contact upon request.

ACKNOWLEDGMENTS

This study is supported by the National Institutes of Health Intramural Research Program and Lasker Clinical Research Scholars Program. T.S.G. is supported by grants from the Washington Research Foundation grant (P1-0346) and Ben and Catherine Ivy Foundation. The authors are grateful for Cothera Biosciences for providing zotiraciclib and for their generous support for brain tumor research. The authors thank Yolanda L. Jones, National Institutes of Health Library, for editing assistance.

AUTHOR CONTRIBUTIONS

Conceptualization, J.W. and Y.P.; methodology, J.W., Y.P., Q.L., G.Y., Z.S., O.K., P.L., M.C., F.J.N., M.M.G., M.G.C., Z.L., J.K., C.J.T., and T.S.G.; investigation, J.W., Y.P., Q.L., G.Y., O.K., P.L., M.C., Z.S., X.S., H.W., A.R., R.W.R., F.S., B.T., F. J. N., M.Z., H.S. W.Z., D.D., and T.S.G.; statistical analyses, J.W., Y.P., Z.S., and T.G.; writing – original draft, J.W. and Y.P.; writing – review and editing, J.W., Y.P., Q.L., Z.S., O.K., P.L., M.C., R.W.R., M.R.G., M.M.G., M.G.C., C.J.T., and T.S.G.; funding acquisition, T.S.G and J.W.; supervision, J.W. All authors read and approved the final article and take responsibility for its content.

DECLARATION OF INTERESTS

The authors declare no competing interests.

STAR★METHODS

Detailed methods are provided in the online version of this paper and include the following:

SUPPLEMENTAL INFORMATION

Supplemental information can be found online at https://doi.org/10.1016/j.isci.2025.112283.

Received: January 2, 2024
Revised: August 7, 2024
Accepted: March 20, 2025
Published: March 25, 2025

REFERENCES

1. van den Bent, M.J., Tesileanu, C.M.S., Wick, W., Sanson, M., Brandes, A.A., Clement, P.M., Erridge, S., Vogelbaum, M.A., Nowak, A.K., Baurain, J.F., et al. (2021). Adjuvant and concurrent temozolomide for 1p/19q non-co-deleted anaplastic glioma (CATNON; EORTC study 26053-22054): second interim analysis of a randomised, open-label, phase 3 study. Lancet Oncol. *22*, 813–823. https://doi.org/10.1016/S1470-2045(21)00090-5.
2. Yan, H., Parsons, D.W., Jin, G., McLendon, R., Rasheed, B.A., Yuan, W., Kos, I., Batinic-Haberle, I., Jones, S., Riggins, G.J., et al. (2009). IDH1 and IDH2 mutations in gliomas. N. Engl. J. Med. *360*, 765–773. https://doi.org/10.1056/NEJMoa0808710.
3. Badur, M.G., Muthusamy, T., Parker, S.J., Ma, S., McBrayer, S.K., Cordes, T., Magana, J.H., Guan, K.L., and Metallo, C.M. (2018). Oncogenic R132 IDH1 Mutations Limit NADPH for De Novo Lipogenesis through (D)2-Hydroxyglutarate Production in Fibrosarcoma Sells. Cell Rep. *25*, 1018–1026.e4. https://doi.org/10.1016/j.celrep.2018.09.074.
4. Dang, L., Jin, S., and Su, S.M. (2010). IDH mutations in glioma and acute myeloid leukemia. Trends Mol. Med. *16*, 387–397. https://doi.org/10.1016/j.molmed.2010.07.002.
5. Fack, F., Tardito, S., Hochart, G., Oudin, A., Zheng, L., Fritah, S., Golebiewska, A., Nazarov, P.V., Bernard, A., Hau, A.C., et al. (2017). Altered metabolic landscape in IDH-mutant gliomas affects phospholipid, energy, and oxidative stress pathways. EMBO Mol. Med. *9*, 1681–1695. https://doi.org/10.15252/emmm.201707729.
6. Miller, J.J., Gonzalez Castro, L.N., McBrayer, S., Weller, M., Cloughesy, T., Portnow, J., Andronesi, O., Barnholtz-Sloan, J.S., Baumert, B.G., Berger, M.S., et al. (2023). Isocitrate dehydrogenase (IDH) mutant gliomas: A Society for Neuro-Oncology (SNO) consensus review on diagnosis, management, and future directions. Neuro Oncol. *25*, 4–25. https://doi.org/10.1093/neuonc/noac207.
7. Nunez, F.J., Mendez, F.M., Kadiyala, P., Alghamri, M.S., Savelieff, M.G., Garcia-Fabiani, M.B., Haase, S., Koschmann, C., Calinescu, A.A., Kamran, N., et al. (2019). IDH1-R132H acts as a tumor suppressor in glioma

via epigenetic up-regulation of the DNA damage response. Sci. Transl. Med. *11*, eaaq1427. https://doi.org/10.1126/scitranslmed.aaq1427.

8. Goh, K.C., Novotny-Diermayr, V., Hart, S., Ong, L.C., Loh, Y.K., Cheong, A., Tan, Y.C., Hu, C., Jayaraman, R., William, A.D., et al. (2012). TG02, a novel oral multi-kinase inhibitor of CDKs, JAK2 and FLT3 with potent anti-leukemic properties. Leukemia *26*, 236–243. https://doi.org/10.1038/leu.2011.218.

9. Wu, J., Yuan, Y., Long Priel, D.A., Fink, D., Peer, C.J., Sissung, T.M., Su, Y.T., Pang, Y., Yu, G., Butler, M.K., et al. (2021). Phase I Study of Zotiraciclib in Combination with Temozolomide for Patients with Recurrent High-grade Astrocytomas. Clin. Cancer Res. *27*, 3298–3306. https://doi.org/10.1158/1078-0432.CCR-20-4730.

10. Roboz, G.J., Khoury, H.J., Shammo, J.M., Syto, M., Burrows, F., Zaknoen, S.L., and Jabbour, E. (2012). Phase I dose escalation study of TG02 in patients with advanced hematologic malignancies. J. Clin. Oncol. *30*, 6577.

11. Su, Y.T., Chen, R., Wang, H., Song, H., Zhang, Q., Chen, L.Y., Lappin, H., Vasconcelos, G., Lita, A., Maric, D., et al. (2018). Novel Targeting of Transcription and Metabolism in Glioblastoma. Clin. Cancer Res. *24*, 1124–1137. https://doi.org/10.1158/1078-0432.CCR-17-2032.

12. Mathews Griner, L.A., Guha, R., Shinn, P., Young, R.M., Keller, J.M., Liu, D., Goldlust, I.S., Yasgar, A., McKnight, C., Boxer, M.B., et al. (2014). High-throughput combinatorial screening identifies drugs that cooperate with ibrutinib to kill activated B-cell-like diffuse large B-cell lymphoma cells. Proc. Natl. Acad. Sci. USA *111*, 2349–2354. https://doi.org/10.1073/pnas.1311846111.

13. Lin, G.L., Wilson, K.M., Ceribelli, M., Stanton, B.Z., Woo, P.J., Kreimer, S., Qin, E.Y., Zhang, X., Lennon, J., Nagaraja, S., et al. (2019). Therapeutic strategies for diffuse midline glioma from high-throughput combination drug screening. Sci. Transl. Med. *11*, eaaw0064. https://doi.org/10.1126/scitranslmed.aaw0064.

14. Wager, T.T., Hou, X., Verhoest, P.R., and Villalobos, A. (2010). Moving beyond rules: the development of a central nervous system multiparameter optimization (CNS MPO) approach to enable alignment of druglike properties. ACS Chem. Neurosci. *1*, 435–449. https://doi.org/10.1021/cn100008c.

15. Wager, T.T., Hou, X., Verhoest, P.R., and Villalobos, A. (2016). Central Nervous System Multiparameter Optimization Desirability: Application in Drug Discovery. ACS Chem. Neurosci. *7*, 767–775. https://doi.org/10.1021/acschemneuro.6b00029.

16. Gottesman, M.M., Lavi, O., Hall, M.D., and Gillet, J.P. (2016). Toward a Better Understanding of the Complexity of Cancer Drug Resistance. Annu. Rev. Pharmacol. Toxicol. *56*, 85–102. https://doi.org/10.1146/annurev-pharmtox-010715-103111.

17. Kim, O., Butler, M., Sergi, Z., Robey, R.W., Zhang, M., Chari, R., Pang, Y., Yu, G., Zhang, W., Song, H., et al. (2023). Combined inhibition of topoisomerase I and poly(ADP-ribose) polymerase: A synergistic therapeutic strategy for glioblastoma with phosphatase and tensin homolog deficiency. Neurooncol. Adv. *5*, vdad102. https://doi.org/10.1093/noajnl/vdad102.

18. Horowitz, L.F., Rodriguez, A.D., Au-Yeung, A., Bishop, K.W., Barner, L.A., Mishra, G., Raman, A., Delgado, P., Liu, J.T.C., Gujral, T.S., et al. (2021). Microdissected "cuboids" for microfluidic drug testing of intact tissues. Lab Chip *21*, 122–142. https://doi.org/10.1039/d0lc00801j.

19. Sivakumar, R., Chan, M., Shin, J.S., Nishida-Aoki, N., Kenerson, H.L., Elemento, O., Beltran, H., Yeung, R., and Gujral, T.S. (2019). Organotypic tumor slice cultures provide a versatile platform for immuno-oncology and drug discovery. OncoImmunology *8*, e1670019. https://doi.org/10.1080/2162402X.2019.1670019.

20. Szulzewsky, F., Arora, S., Arakaki, A.K.S., Sievers, P., Almiron Bonnin, D.A., Paddison, P.J., Sahm, F., Cimino, P.J., Gujral, T.S., and Holland, E.C. (2022). Both YAP1-MAML2 and constitutively active YAP1 drive the formation of tumors that resemble NF2 mutant meningiomas in mice. Genes Dev. *36*, 857–870. https://doi.org/10.1101/gad.349876.122.

21. Grassian, A.R., Parker, S.J., Davidson, S.M., Divakaruni, A.S., Green, C.R., Zhang, X., Slocum, K.L., Pu, M., Lin, F., Vickers, C., et al. (2014). IDH1 mutations alter citric acid cycle metabolism and increase dependence on oxidative mitochondrial metabolism. Cancer Res. *74*, 3317–3331. https://doi.org/10.1158/0008-5472.CAN-14-0772-T.

22. Reitman, Z.J., Jin, G., Karoly, E.D., Spasojevic, I., Yang, J., Kinzler, K.W., He, Y., Bigner, D.D., Vogelstein, B., and Yan, H. (2011). Profiling the effects of isocitrate dehydrogenase 1 and 2 mutations on the cellular metabolome. Proc. Natl. Acad. Sci. USA *108*, 3270–3275. https://doi.org/10.1073/pnas.1019393108.

23. Le Rhun, E., von Achenbach, C., Lohmann, B., Silginer, M., Schneider, H., Meetze, K., Szabo, E., and Weller, M. (2019). Profound, durable and MGMT-independent sensitivity of glioblastoma cells to cyclin-dependent kinase inhibition. Int. J. Cancer *145*, 242–253. https://doi.org/10.1002/ijc.32069.

24. Olsen, R.K.J., Cornelius, N., and Gregersen, N. (2015). Redox signalling and mitochondrial stress responses; lessons from inborn errors of metabolism. J. Inherit. Metab. Dis. *38*, 703–719. https://doi.org/10.1007/s10545-015-9861-5.

25. Yakovlev, G., and Hirst, J. (2007). Transhydrogenation reactions catalyzed by mitochondrial NADH-ubiquinone oxidoreductase (Complex I). Biochemistry *46*, 14250–14258. https://doi.org/10.1021/bi7017915.

26. Tateishi, K., Wakimoto, H., Iafrate, A.J., Tanaka, S., Loebel, F., Lelic, N., Wiederschain, D., Bedel, O., Deng, G., Zhang, B., et al. (2015). Extreme Vulnerability of IDH1 Mutant Cancers to NAD+ Depletion. Cancer Cell *28*, 773–784. https://doi.org/10.1016/j.ccell.2015.11.006.

27. Yaku, K., Okabe, K., and Nakagawa, T. (2018). NAD metabolism: Implications in aging and longevity. Ageing Res. Rev. *47*, 1–17. https://doi.org/10.1016/j.arr.2018.05.006.

28. Guo, C., Sun, L., Chen, X., and Zhang, D. (2013). Oxidative stress, mitochondrial damage and neurodegenerative diseases. Neural Regen. Res. *8*, 2003–2014. https://doi.org/10.3969/j.issn.1673-5374.2013.21.009.

29. Gelman, S.J., Naser, F., Mahieu, N.G., McKenzie, L.D., Dunn, G.P., Chheda, M.G., and Patti, G.J. (2018). Consumption of NADPH for 2-HG Synthesis Increases Pentose Phosphate Pathway Flux and Sensitizes Cells to Oxidative Stress. Cell Rep. *22*, 512–522. https://doi.org/10.1016/j.celrep.2017.12.050.

30. Clarke, D.J.B., Kuleshov, M.V., Schilder, B.M., Torre, D., Duffy, M.E., Keenan, A.B., Lachmann, A., Feldmann, A.S., Gundersen, G.W., Silverstein, M.C., et al. (2018). eXpression2Kinases (X2K) Web: linking expression signatures to upstream cell signaling networks. Nucleic Acids Res. *46*, W171–W179. https://doi.org/10.1093/nar/gky458.

31. Warfel, N.A., and Kraft, A.S. (2015). PIM kinase (and Akt) biology and signaling in tumors. Pharmacol. Ther. *151*, 41–49. https://doi.org/10.1016/j.pharmthera.2015.03.001.

32. Berger, S.I., Posner, J.M., and Ma'ayan, A. (2007). Genes2Networks: connecting lists of gene symbols using mammalian protein interactions databases. BMC Bioinformatics *8*, 372. https://doi.org/10.1186/1471-2105-8-372.

33. van der Lugt, N.M., Domen, J., Verhoeven, E., Linders, K., van der Gulden, H., Allen, J., and Berns, A. (1995). Proviral tagging in E mu-myc transgenic mice lacking the Pim-1 proto-oncogene leads to compensatory activation of Pim-2. EMBO J. *14*, 2536–2544. https://doi.org/10.1002/j.1460-2075.1995.tb07251.x.

34. Hoover, D., Friedmann, M., Reeves, R., and Magnuson, N.S. (1991). Recombinant human pim-1 protein exhibits serine/threonine kinase activity. J. Biol. Chem. *266*, 14018–14023.

35. Bellon, M., and Nicot, C. (2023). Targeting Pim kinases in hematological cancers: molecular and clinical review. Mol. Cancer *22*, 18. https://doi.org/10.1186/s12943-023-01721-1.

36. Luszczak, S., Kumar, C., Sathyadevan, V.K., Simpson, B.S., Gately, K.A., Whitaker, H.C., and Heavey, S. (2020). PIM kinase inhibition: co-targeted

therapeutic approaches in prostate cancer. Signal Transduct. Target. Ther. *5*, 7. https://doi.org/10.1038/s41392-020-0109-y.

37. Chauhan, S.S., Toth, R.K., Jensen, C.C., Casillas, A.L., Kashatus, D.F., and Warfel, N.A. (2020). PIM kinases alter mitochondrial dynamics and chemosensitivity in lung cancer. Oncogene *39*, 2597–2611. https://doi.org/10.1038/s41388-020-1168-9.
38. Yu, G., Pang, Y., Merchant, M., Kesserwan, C., Gangalapudi, V., Abdelmaksoud, A., Ranjan, A., Kim, O., Wei, J.S., Chou, H.C., et al. (2021). Tumor Mutation Burden, Expressed Neoantigens and the Immune Microenvironment in Diffuse Gliomas. Cancers *13*, 6092. https://doi.org/10.3390/cancers13236092.
39. Navis, A.C., Niclou, S.P., Fack, F., Stieber, D., van Lith, S., Verrijp, K., Wright, A., Stauber, J., Tops, B., Otte-Holler, I., et al. (2013). Increased mitochondrial activity in a novel IDH1-R132H mutant human oligodendroglioma xenograft model: in situ detection of 2-HG and alpha-KG. Acta Neuropathol. Commun. *1*, 18. https://doi.org/10.1186/2051-5960-1-18.
40. Harrision, D., Gravells, P., Thompson, R., and Bryant, H.E. (2020). Poly(-ADP-Ribose) Glycohydrolase (PARG) vs. Poly(ADP-Ribose) Polymerase (PARP) - Function in Genome Maintenance and Relevance of Inhibitors for Anti-cancer Therapy. Front. Mol. Biosci. *7*, 191. https://doi.org/10.3389/fmolb.2020.00191.
41. Fernandez-Marcos, P.J., and Nóbrega-Pereira, S. (2016). NADPH: new oxygen for the ROS theory of aging. Oncotarget *7*, 50814–50815. https://doi.org/10.18632/oncotarget.10744.
42. Dang, L., White, D.W., Gross, S., Bennett, B.D., Bittinger, M.A., Driggers, E.M., Fantin, V.R., Jang, H.G., Jin, S., Keenan, M.C., et al. (2009). Cancer-associated IDH1 mutations produce 2-hydroxyglutarate. Nature *462*, 739–744. https://doi.org/10.1038/nature08617.
43. Ward, P.S., Patel, J., Wise, D.R., Abdel-Wahab, O., Bennett, B.D., Coller, H.A., Cross, J.R., Fantin, V.R., Hedvat, C.V., Perl, A.E., et al. (2010). The common feature of leukemia-associated IDH1 and IDH2 mutations is a neomorphic enzyme activity converting alpha-ketoglutarate to 2-hydroxyglutarate. Cancer Cell *17*, 225–234. https://doi.org/10.1016/j.ccr.2010.01.020.
44. Rushmore, T.H., Morton, M.R., and Pickett, C.B. (1991). The antioxidant responsive element. Activation by oxidative stress and identification of the DNA consensus sequence required for functional activity. J. Biol. Chem. *266*, 11632–11639.
45. Inoue, S., Li, W.Y., Tseng, A., Beerman, I., Elia, A.J., Bendall, S.C., Lemonnier, F., Kron, K.J., Cescon, D.W., Hao, Z., et al. (2016). Mutant IDH1 Downregulates ATM and Alters DNA Repair and Sensitivity to DNA Damage Independent of TET2. Cancer Cell *30*, 337–348. https://doi.org/10.1016/j.ccell.2016.05.018.
46. Turcan, S., Makarov, V., Taranda, J., Wang, Y., Fabius, A.W.M., Wu, W., Zheng, Y., El-Amine, N., Haddock, S., Nanjangud, G., et al. (2018). Mutant-IDH1-dependent chromatin state reprogramming, reversibility, and persistence. Nat. Genet. *50*, 62–72. https://doi.org/10.1038/s41588-017-0001-z.
47. Akalin, A., Garrett-Bakelman, F.E., Kormaksson, M., Busuttil, J., Zhang, L., Khrebtukova, I., Milne, T.A., Huang, Y., Biswas, D., Hess, J.L., et al. (2012). Base-pair resolution DNA methylation sequencing reveals profoundly divergent epigenetic landscapes in acute myeloid leukemia. PLoS Genet. *8*, e1002781. https://doi.org/10.1371/journal.pgen.1002781.
48. Rohle, D., Popovici-Muller, J., Palaskas, N., Turcan, S., Grommes, C., Campos, C., Tsoi, J., Clark, O., Oldrini, B., Komisopoulou, E., et al. (2013). An inhibitor of mutant IDH1 delays growth and promotes differentiation of glioma cells. Science *340*, 626–630. https://doi.org/10.1126/science.1236062.
49. Ma, D., Zhan, D., Fu, Y., Wei, S., Lal, B., Wang, J., Li, Y., Lopez-Bertoni, H., Yalcin, F., Dzaye, O., et al. (2021). Mutant IDH1 promotes phagocytic function of microglia/macrophages in gliomas by downregulating ICAM1. Cancer Lett. *517*, 35–45. https://doi.org/10.1016/j.canlet.2021.05.038.
50. Kim, O., Sergi, Z., Yu, G., Yamamoto, K., Quezado, M., Abdullaev, Z., Crooks, D.R., Kishimoto, S., Li, Q., Lu, P., et al. (2024). A patient-derived cell model for malignant transformation in IDH-mutant glioma. Acta Neuropathol. Commun. *12*, 148. https://doi.org/10.1186/s40478-024-01860-6.
51. Anastassiadis, T., Deacon, S.W., Devarajan, K., Ma, H., and Peterson, J.R. (2011). Comprehensive assay of kinase catalytic activity reveals features of kinase inhibitor selectivity. Nat. Biotechnol. *29*, 1039–1045. https://doi.org/10.1038/nbt.2017.
52. Jha, P., Wang, X., and Auwerx, J. (2016). Analysis of Mitochondrial Respiratory Chain Supercomplexes Using Blue Native Polyacrylamide Gel Electrophoresis (BN-PAGE). Curr. Protoc. Mouse Biol. *6*, 1–14. https://doi.org/10.1002/9780470942390.mo150182.
53. Greer, Y.E., Porat-Shliom, N., Nagashima, K., Stuelten, C., Crooks, D., Koparde, V.N., Gilbert, S.F., Islam, C., Ubaldini, A., Ji, Y., et al. (2018). ONC201 kills breast cancer cells in vitro by targeting mitochondria. Oncotarget *9*, 18454–18479. https://doi.org/10.18632/oncotarget.24862.
54. Tilghman, J., Schiapparelli, P., Lal, B., Ying, M., Quinones-Hinojosa, A., Xia, S., and Laterra, J. (2016). Regulation of Glioblastoma Tumor-Propagating Cells by the Integrin Partner Tetraspanin CD151. Neoplasia *18*, 185–198. https://doi.org/10.1016/j.neo.2016.02.003.

STAR★METHODS

KEY RESOURCES TABLE

REAGENT or RESOURCE	SOURCE	IDENTIFIER
Antibodies		
p-RNA POLII	Abcam	#ab5095; RRID: AB_304749
p-CDK9	Cell signaling technology (CST)	#2549; RRID: AB_2077300
CDK9	CST	#2316; RRID: AB_2291505
cleaved-caspase 3	CST	#9661; RRID: AB_2341188
γ-H2A.X	CST	#9718; RRID: AB_2118009
cleaved-PARP	CST	#5625; RRID: AB_10699459
MCL-1	CST	#5453; RRID: AB_10694494
XIAP	CST	#14334; RRID: AB_2784533
survivin	CST	#2808; RRID: AB_2063948
cleaved-caspase 8	CST	#9496; RRID: AB_561381
cleaved-caspase 9	CST	#7237; RRID: AB_10895832
LC3B	CST	#3868; RRID: AB_2137707
NAMPT	Abcam	#ab236873; RRID: AB_3678661
NAPRT1	Abcam	#ab211529; RRID: AB_3678660
G6PG	CST	#8866; RRID: AB_10827744
PGD	CST	#13389; RRID: AB_2798202
GAPDH	CST	#5174; RRID: AB_10622025
β-actin	CST	#8457; RRID: AB_10950489
Phospho-PIM1/3	Invitrogen	#PA5-37683; RRID: AB_2554291
PIM1	CST	#3247; RRID: AB_2299591
PIM3	CST	#4165; RRID: AB_1904094
PIM1 (IHC)	ABclonal	#A19695; RRID: AB_2862740
Chemicals, peptides, and recombinant proteins		
ZTR	Cothera Bioscience	NA
Z-VAD	BD Biosciences	# 550377
Critical commercial assays		
ROS-Glo H_2O_2 assay kit	Promega	G8820
Caspase-Glo 3/7 Assay Kit	Promega	G8091
Seahorse XF Cell Mito Stress Test Kit	Agilent	103015-100
Seahorse XF Real-Time ATP Rate Assay Kit	Agilent	103592-100
NAMPT Activity Assay Kit	Abcam	ab221819
NAD/NADH-Glo Assay Kit	Promega	G9071
NADP/NADPH-Glo Assay Kit	Promega	G9081
MycoAlert Mycoplasma Detection Kit	Lonza	#LT07-318
Deposited data		
Raw and processed RNA sequencing data	This paper	GEO: GSE252245
Experimental models: Cell lines		
GSC923	NOB/NCI	NA
GSC827	NOB/NCI	NA
TS603	Dr. Timothy Chan, Memorial Sloan Kettering Cancer Center, New York, NY	NA
BT142	ATCC	ACS-1018

(*Continued on next page*)

Continued		
REAGENT or RESOURCE	SOURCE	IDENTIFIER
GSC403L/H	NOB/NCI	NA
MGG152	Dr. Daniel Cahill, The General Hospital Corp. d/b/a/ Massachusetts General Hospital, 55 Fruit Street Boston, MA	NA
SF10602	Dr. Joseph F Costello, Department of Neurological Surgery, University of California, San Francisco, CA	NA
NPA/NPAI	Dr. Maria G. Castro, University of Michigan Medical School, Ann Arbor, MI	NA
$U87^{wt}$, $U87^{C8}$ (IDH-mutant) and $U87^{C44}$ (IDH-mutant)	Dr. Shuli Xia, Johns Hopkins University School of Medicine, Baltimore, MD	NA
$GBM1^{wt}$ and $GBM1^{mut}$ (IDH-mutant))	Dr. Shuli Xia, Johns Hopkins University School of Medicine, Baltimore, MD	NA
Experimental models: Organisms/strains		
C57BL/6 albino mice	Charles river lab	562
Athymic (nu/nu) mice	NCIs BTB	NA
Software and algorithms		
GraphPad Prism 9 software	GraphPad	9.2.0 (283)
ImageJ software	Fiji	1.54f

EXPERIMENTAL MODEL AND STUDY PARTICIPANT DETAILS

Cell lines and primary cells

GSC923 and GSC827 were generated from patients' glioblastoma tissues in NOB/NCI laboratory.[11] GSC923 has an unmethylated MGMT promotor, which GSC827 exhibit a methylated MGMT promotor. TS603, a patient-derived high-grade astrocytoma cell line, was obtained from Dr. Timothy Chan, Memorial Sloan Kettering Cancer Center, New York, NY.[48] BT142, a patient-derived oligoastrcytoma cell line, was purchased from ATCC. NPA (shp53/shATRX/wtIDH1) and NPAI (shp53/shATRX/mIDH1^{R132H}), mice-derived neurosphere cell lines, were provided by Dr. Maria G. Castro, University of Michigan Medical School, Ann Arbor, MI.[7] Isogenic U87 ($U87^{wt}$, $U87^{C8}$ (IDH-mutant) and $U87^{C44}$ (IDH-mutant)) and GBM1, patient-derived glioblastoma cell lines, ($GBM1^{wt}$ and $GBM1^{mut}$ (IDH-mutant)) cell lines were provided by Dr. Shuli Xia, Johns Hopkins University School of Medicine, Baltimore, MD.[49] GSC403L and GSC403H cell lines were generated in NOB/NCI laboratory. 403L tumor tissue sample was obtained at WHO grade 2, while 403H sample was obtained from the same patient when the tumor transformed to WHO grade 4.[50] All the patient-derived stem-like cell lines and their key molecular features were summarized in Table S3. The glioma stem-like cells (GSC923, GSC827, TS603, BT142, GSC403L, GSC403H, NPA, NPAI, and GBM1) were cultured in 3D environment containing neurobasal-A medium or DMEM/F12 medium supplemented with bFGF, EGF, N2, B27, and penicillin/streptomycin at 37°C with 5% CO_2. Adherent cell lines (U251 and HT1080) were purchased from the ATCC and 2D cultured in DMEM medium supplemented with 10% FBS and 1% Penicillin/Streptomycin. The cell lines GSC923, GSC827, TS603, NPA, NPAI, isogenic U87 (U87wt, U87C8, and U87C44), GBM1wt, GBM1mut, GSC403L, and GSC403H have been authenticated in previously published studies.[7,11,48–50] All cells were routinely checked for mycoplasma contamination using MycoAlert Mycoplasma kit (Lonza, Walkersville, MD, USA).

Mice and ethics statement

Eight-week-old female C57BL/6 albino mice were used to establish the syngeneic NPA/NPAI model, while seven-week-old female athymic (nu/nu) mice were used for the xenograft orthotopic model. All the animal experiments were reviewed and approved by the National Cancer Institute Animal Care and Use Committee (NCI ACUC) and conducted in accordance with NCI ACUC guidelines under the authority of the animal protocol (NOB-023).

Patient-derived organotypic tumor specimens

Fresh surgical specimens were collected from the patient undergoing surgical resection of the tumor at the Surgical Neurology Branch (SNB) at National Institutes of Health (NIH). The research was approved by the Institutional Review Board at NIH (SNB 03N0164). Written informed consent for the study was obtained from the patient. The patients' demographic features and clinical information were summarized in Table S4.

METHOD DETAILS

Kinase inhibition assay

In vitro kinase panel profiling was performed using the "HotSpot" assay platform by Reaction Biology Corp as described previously.[51] Briefly, kinase, substrate, and cofactors were prepared in reaction buffer at room temperature. ZTR at 500 nM, ATP and 33P ATP was added to a final concentration of 10 μM. Reaction spotting was performed using ion exchange filter paper. Any unbound phosphate was eliminated with phosphoric acid. The kinase activity results were reported as the percentage of remaining kinase activity in ZTR samples relative to the vehicle control.

Cell viability assay

Cells were growing in 3D culture. A total of 1×10^5 cells/well were plated as 2D culture in geltrex precoated 12-well plates and treated with ZTR for 72 hours prior to cell counting using a Beckman Coulter ViCELL TM XR cell viability analyzer or Celigo Imaging Cytometer (Nexcelom Bioscience).

High throughput single agent screening

Six patient-derived glioma stem-like cell lines with *IDH1* mutations (GSC403L, GSC403H, BT142, MGG152, SF10602, and TS603) were screened with a cytotoxicity assay (48 hours Cell Titer-Glo) versus the MIPE 5.0 library (2,481 agents: approved and investigational drugs with known MOA), as described and reported previously.[12,13] AUC was utilized for ranking drug potency. For each compound tested, AUC values were averaged across the six cell lines and then normalized to Z-scores. MPO scores were plotted against Z-scores. Compounds of interest were highlighted based on an MPO score greater than 4 and an AUC Z-score of less than -3.

ROS measurement

ROS was measured using ROS-Glo H_2O_2 assay kit (Promega). Briefly, cells were maintained in 3D culture. 1×10^4 cells/well were plated in geltrex precoated 96-well plates and treated with ZTR. H_2O_2 substrate solution was added in the culture medium and incubated for 6 hours. After adding ROS-Glo detection solution and incubating for 20 minutes, luminescence signal was read by the POLARStar Optima plate reader. The raw value was normalized to the protein content.

Caspase 3/7 activity assay

Caspase 3/7 cleavage activity was measured by Caspase-Glo 3/7 Assay Kit (Promega). Cells were plated as 2D culture in a precoated 96-well plate. After treatment with ZTR for 72 hours, all wells were incubated with an equal volume of Caspase-Glo 3/7 reagent for 30 minutes and the luminescence signal was read by POLARStar Optima plate reader.

Cell apoptosis assay

The cells were maintained and treated in 3D culture. ZTR-treated cells were differentially stained with APC Annexin V (BD Biosciences) and propidium iodide (PI) followed by flow cytometry analysis performed based on the manufacturer's protocol. The fluorescence signal was measured by an BD LSRFortessa SORP I flow cytometer within 1 hour of staining and the percentage of apoptotic cells was quantified by FlowJo.

Western blot

Cells were maintained and treated with ZTR at 15 nM in 3D culture prior to the cell harvest. The cell lysates were processed with ice-cold RIPA lysis buffer supplemented with protease and phosphatase Inhibitor Cocktail (Thermo Fisher Scientific). Protein concentration was determined by a DC Protein Assay kit (Bio-Rad) and the same amount of protein was resolved by NuPAGE 4% - 12% Noves Bis-Tris gels (Invitrogen). Proteins were transferred to nitrocellulose membranes (Bio-Rad) and probed with primary antibodies (diluted 1:1000) at 4°C overnight. After secondary antibody incubation and washing, membranes were visualized using ChemiDoc imaging system (Bio-Rad).

DNA fragmentation assay

Two million 3D cultured cells were treated with DMSO or 15 nM of ZTR for 48 hours. DNA was extracted using the DNeasy Blood & Tissue kit (Qiagen) and total DNA concentration was determined by NanoDrop 8-Sample Spectrophotometer. Five hundred nanogram of DNA samples were resolved by electrophoresis in 10% Novex TBE gel (Invitrogen). The gel was stained by SYBR Gold DNA dye for 20 minutes and visualized by the ChemiDoc Imaging system (Bio-Rad).

MitoTracker green FM staining

Cells previously growing in 3D culture were seeded in pre-coated 8-well glass coverslip (BD Biosciences) and treated with DMSO or 15 nM ZTR for 48 hours. After removing media from the coverslip, prewarmed staining solution with MitoTracker Green FM (100 nM, Thermo Fisher Scientific) was added for 30 minutes incubation at 37°C. After staining nuclei with Hoechst 33342, cells were observed using a NIKON confocal microscope. The area of fluorescence of each single cell was determined using ImageJ software (Version 1.54f, Bethesda, MD).

Blue native polyacrylamide gel electrophoresis and complex I in-gel activity assay

Cells were maintained and treated in 3D culture. They were then and collected, washed with PBS, and homogenized in the sample buffer, supplemented with 1% digitonin. After centrifuging the cell lysate at 20,000 g for 30 min at 4°C, supernatant was collected and aliquoted for further assay. Protein concentration was measured by the DC Protein Assay kit (Bio-Rad) and the same amount of sample was mixed with sample buffer, 5% G-250 Sample Additive, and deionized water for native gel electrophoresis in dark blue cathode buffer. When gel electrophoresis was done, the gel was fixed in 40% methanol, 10% acetic acid buffer, and then the gel was washed in destain buffer (8% acetic acid) until the background was washed off for visualization by ChemiDoc Imaging system (Bio-Rad).

For Complex I in-gel activity assay, after gel electrophoresis in light blue cathode buffer, the gel was incubated in fresh Complex I substrate buffer (2 mM Tris·Cl, 0.1 mg/ml NADH, 2.5 mg/ml Nitrotetrazolium Blue chloride) for 20 min.[52] The reaction was stopped by 10% acetic acid and the gel was washed with water for visualization by ChemiDoc Imaging system (Bio-Rad).

Mitochondrial respiration and ATP real-time measurement assay

Mitochondria respiration and real-time ATP production was assessed by Seahorse XF Cell Mito Stress Test Kit (Agilent) and Seahorse XF Real-Time ATP Rate Assay Kit (Agilent), respectively. Briefly, cells previously maintained in 3D culture were plated at a density of 40,000 cells/well in the precoated Seahorse cell culture plates per manufacturer's manual. After cells were attached and stabilized, cells were treated with DMSO or ZTR for 24 hours. Medium in all wells was replaced by the XF based assay medium supplemented with 10mM glucose, 10mM sodium pyruvate and 2mM glutamine. After loading to the Seahorse XF96 analyzer (Agilent), compounds included in the Mito Stress Test Kit (oligomycin, FCCP and Rot/AA) or Real-Time ATP Rate Assay Kit (oligomycin and Rot/AA) were injected according to the pre-set programs for measurement.

NAD and NADP assay

NAD(H) and NADP(H) levels were measured by NAD/NADH-Glo and NADP/NADPH-Glo kits (Promega), respectively. NPA/NPAI cell lines, previously maintained in 3D culture, were seeded on precoated 96 well plates and treated with 50 nM ZTR for 48 hours. GSC cell lines (GSC923, GSC827, TS603, and BT142) were seeded as 2D culture in 96 well plates and treated with 15 nM ZTR for 48 hours. At the end of ZTR treatment, all wells were processed following the instructions of the assay kits and luminescence output was measured using a luminometer. The raw value was normalized to the protein content.

NAMPT activity assay

Cell-free NAMPT activity assay was performed using NAMPT Activity Assay Kit (Abcam) following the manufacturer's instructions. Briefly, ZTR was diluted to 0, 20, 30, 40, and 50 nM, and FK866 (0.4 mM) was used as the control inhibitor. After all reactions were assembled following the instruction, output was measured at OD 450 nm on a microplate reader in kinetic mode, every 5 minutes, for 60 minutes protected from light.

Transmission electron microscope assay

GSC923 and TS603 cells were treated with DMSO or 15nM ZTR for 48 hours treatment in 3D culture for further TEM assay as previously described.[53] Briefly, each sample in an individual well in the form of adherent cells was pre-fixed prior to be processed for TEM analysis. All samples were stained with 1% Osmium Tetroxide and 0.5% Uranyl Acetate successively. And then all samples were dehydrated and kept in 100% pure resin for infiltration overnight. Samples would be polymerized, and ultra-thin sectioned with Leica UC6 Microtome with 70 - 80 nm thickness and picked up on 150-Cu mesh grid. Following post-staining with 50:50 (0.5% Uranyl Acetate:70% Ethanol), samples would be carbon coated and then imaged by Hitachi TEM microscope H7600, with bottom mount camera at HV: 80.0kv for TEM analysis.

RNA sequencing

GSC923 and TS603 cells were 3D cultured and treated with DMSO or 15 nM ZTR and collected after 24 or 48 hours. Total RNA was extracted using RNeasy Mini Kit (Qiagen) and passed the quality control of the Agilent RNA ScreenTape system.

mRNA-Seq samples were pooled and sequenced on NextSeq 2000 P3 using TruSeq Stranded mRNA Kit and paired-end sequencing. Reads were aligned to the reference genome hg38 and gene expression levels were quantified using STAR and RSEM tools. The differentially expressed gene (DEG) list was generated via R package edgeR using the expression values from the ZTR treated samples as input and was limited to protein-coding genes with FDR $\leq$ 0.05. The DEG set used for GO bioprocess pathway enrichment plot were further filtered with the following filtering criteria: logCPM $\geq$ 0 and absolute logFC value $\geq$ 1. The up-regulated and downregulated genes were separated and plotted individually. R package cluster Profiler was used to analyze and illustrate the enrichment plots.

Syngeneic and xenograft orthotopic murine models of glioma

Both syngeneic and xenograft orthotopic glioma mouse models were created to evaluate the treatment effect of ZTR in IDH-mutant and IDH-wildtype gliomas. To generate syngeneic model, isogenic cell line NPA (IDH-wt) or NPAI (IDH-mut) were injected (50,000 cells/2 μL) into the striatum of 8-weeks old female C57BL/6 albino mice using a stereotactic device (coordinates, 2 mm anterior

and 2 mm lateral from bregma, and 2.5 mm depth from the dura). Animals bearing IDH-mut and IDH-wildtype tumors were randomized into two groups based on body weights (n = 7 mice for each group). Seven days after tumor implantation, ZTR (30mg/kg, i.p.) was administered twice a week for 21 days. To generate xenograft orthotopic model of gliomas with and without *IDH* mutation, isogenic cell line GBM1-wildtype or GBM1-mutant (500,000 cells/2 μl) were injected into 7-week-old female athymic (nu/nu) mice as previously described.[54] Two weeks after injection, ZTR treatment (30 mg/kg, i.p.) was administered, twice a week for 10 weeks. Animal behavior and body weight were monitored constantly. Animals were euthanized when they reached the endpoints. The experimental endpoint criteria for intracranial tumors include symptoms of increase intracranial pressure such as less moving around the cage and appears drowsy with less response to stimuli; signs of neurological impairment, such as paralysis, circling, head tilting and conclusion; swollen/domed cranium; swelling subcutaneously at injection site >1cm diameter or that adversely affects the general well-being of the mouse. Additional humane endpoint criteria include body weight loss (>15%), rough hair coat, hunched posture, rapid or labored breathing, debilitating diarrhea, dehydration, lethargy, jaundice, pallor or cyanosis, anemia, bleeding from any orifice, self-induced trauma, impaired mobility affecting the ability to reach food or water. Kaplan-Meier analysis was performed to determine the survival curve. Tumor tissues were collected to analyze PD markers after treatment.

Tissue slices and 3D microtumors preparation

Organotypic tumor slices were prepared from human CNS tumors using a Leica VT1200S vibratome as described previously.[18–20] Slices were immersed in ice-cold HBSS during preparation, with vibratome settings of an 18° blade angle, 0.14 mm/s cutting speed, and a 2.0 mm vibration amplitude. To create 3D microtumors, slices were arranged in a monolayer on a plastic disc and sectioned using a McIlwain Tissue Chopper, rotating the disc 90° and repeating the process. 3D microtumors were cultured in Williams' Medium E with various supplements. For drug evaluation, 3D microtumors were treated with Realtime-Glo MT cell viability reagent at 1:1000 dilution in 96-well plates. After 24 hours, luminescence signals were measured using a Biotek Synergy H4 microplate reader. Wells with signals exceeding 10,000 were selected for ZTR treatment in duplicate or triplicate. Luminescence was monitored for 3 to 7 days post-treatment, and viability was determined by the ratio of the signal at the end of the study to the signal before treatment, normalized to the vehicle control (DMSO) value set to 100%.

QUANTIFICATION AND STATISTICAL ANALYSIS

Statistical analysis was performed using GraphPad Prism software using Student's *t*-test or one-way ANOVA test followed by Student's t-test as the post-statistical analysis. All tests were two-sided, and the results were shown as mean ± SEM or SD. For time course data, a two-sample Student's t-test at each time point with the Bonferroni correction was performed. For MitoTracker Green intensity analysis, a two-way ANOVA test was performed. A p-value less than 0.05 was considered statistically significant. *, $p < 0.05$; **, $p < 0.01$; ***, or $p < 0.001$.